

Visco-Elasto-Capillary Thinning and Break-Up of Complex Fluids

Gareth H. McKinley

April 2005
HML Report Number 05-P-04

VISCO-ELASTO-CAPILLARY THINNING AND BREAK-UP OF COMPLEX FLUIDS

Gareth H. McKinley

Hatsopoulos Microfluids Laboratory, Dept. of Mechanical Engineering,
Massachusetts Institute of Technology, Cambridge, MA 02139, USA

ABSTRACT

The progressive break-up of an initially stable fluid column or thread into a number of smaller droplets is an important dynamical process that impacts many commercial operations from spraying and atomization of fertilizers and pesticides, to paint application, roll-coating of adhesives and food processing operations such as container- and bottle-filling. The progressive thinning of a fluid filament is driven by capillarity and resisted by inertia, viscosity and additional stresses resulting from the extensional deformation of the fluid microstructure within the thread. In many processes of interest the fluid undergoing break-up is non-Newtonian and may contain dissolved polymer, suspended particles, surfactants or other microstructural constituents. In such cases the transient extensional viscosity of the fluid plays an important role in controlling the dynamics of break-up. The intimate connection between the degree of strain-hardening that develops during free extensional flow and the dynamical evolution in the profile of a thin fluid thread is also manifested in heuristic concepts such as ‘spinnability’, ‘tackiness’ and ‘stringiness’. In this review we survey recent experimental and theoretical developments in the field of capillary-driven thinning and break-up with a special focus on how quantitative measurements of the thinning and rupture processes can be used to quantify the material properties of the fluid. As a result of the absence of external forcing the dynamics of the necking process are often self-similar and observations of this ‘self-thinning’ can be used to extract qualitative, and even quantitative, measures of the transient extensional viscosity of a complex fluid.

KEYWORDS: Jet break-up; Necking; Capillary thinning; Extensional rheology; drop formation.

1. INTRODUCTION

The uniaxial extensional viscosity is a fundamental material property of a fluid which characterizes the resistance of a material to stretching deformations. For microstructured fluids, this extensional viscosity is a function of both the rate of deformation and the total strain accumulated. Some of the most common

manifestations of extensional viscosity effects in complex fluids are the dramatic changes they have on the lifetime of a fluid thread undergoing capillary break-up. The so-called “beads on a string” morphology that develops when a jet of a dilute solution of high molecular weight polymer undergoes capillary-driven thinning is a well-known example of this phenomenon [1]. The process of break-up is driven by the action of capillarity, which seeks to minimize the interfacial energy of the free surface of a fluid thread or ‘blob’ by formation of spherical droplets. This dynamical process can be very rapid, depending on the composition of the fluid, and viscous, elastic and inertial stresses may all be important in resisting the action of capillarity. In this chapter, we review recent experimental and theoretical developments in the field of capillary-driven break-up with a special focus on how quantitative measurements of the thinning and rupture processes can be used to quantify the material properties of the fluid. As a result of the absence of external forcing, the dynamics of the necking process are often self-similar and observations of this ‘self-thinning’ can be utilized to extract qualitative and even quantitative measures of the transient extensional viscosity of a complex fluid. However, the temporal evolution of the filament profile depends on the relative importance of viscous and elastic contributions to the stress and the capillary pressure within the fluid thread. In order to obtain useful material information, it is thus essential to understand this *visco-elasto-capillary* balance in detail.

1.1 Application Areas

In addition to its use in extensional rheometry, the progressive break-up of an initially stable fluid column or thread into a number of smaller droplets is an important dynamical process that impacts many commercial operations from spraying and atomization of fertilizers and pesticides, to roll-coating and food processing operations such as bottle-filling. The intimate connection between the degree of strain-hardening that develops during free extensional flow and the dynamical evolution in the profile of a thin fluid thread is important in a diverse range of free-surface flows and industrial processing operations such as those shown in figure 1.

The retarded breakup of a high-speed fluid jet containing low concentrations of a high molecular weight additive (such as polyethylene oxide (PEO) in this case) is a well-known example [2] shown in figure 1(a), with applications in drag reduction and fire-hoses [3]. Food-stuffs frequently contain natural (or synthetic) biopolymeric ‘thickeners’ which result in stringiness. Cutting an *okra* (a.k.a ‘ladyfinger’) in half, as shown in figure 1(b), ruptures the cell-walls and releases the cellular cytoplasm which stabilizes the formation of a thin thread as the two halves are separated. Figure 1(c) shows the ‘bag-break up’ atomization process in a fluid droplet of diameter $650\ \mu\text{m}$ (containing 125 ppm of PEO; $M \sim 2 \times 10^6\ \text{g/mol}$) ejected from a nozzle into a high speed cross-stream airflow [4]. The stagnation pressure acting on the nose of the fluid droplet rapidly inverts and inflates it into a stretched fluid shell, which subsequently undergoes capillary breakup. The extensional stresses in the rapidly-stretched fluid sheet lead once again to thin threads and interconnected droplets. The level of fluid viscoelasticity can thus be used to control droplet size and airborne chemical

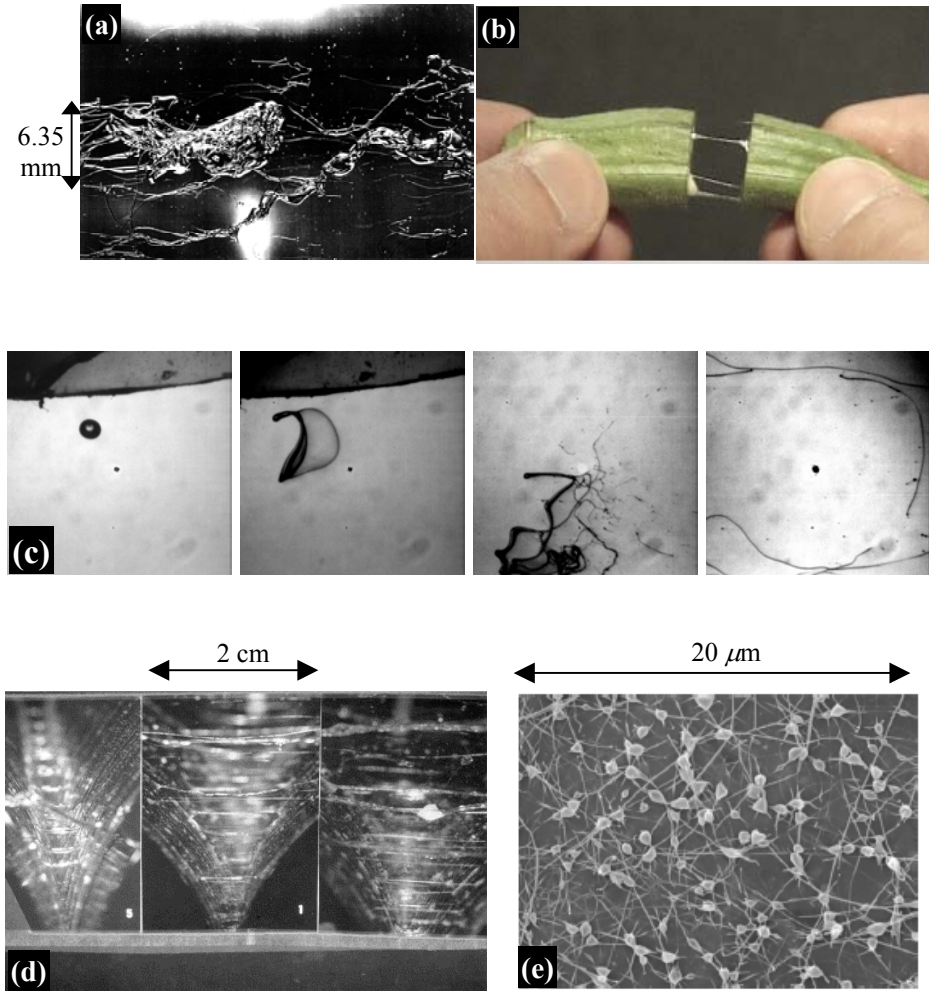


Figure 1: Some common application areas that involve visco-elasto-capillary thinning of a complex fluid; (a) breakup of a fluid jet at high Reynolds number, $Re \approx 35000$, containing a small amount (100ppm) of polyethylene oxide solution (reproduced from Boger & Walters, 1993 [2]; from an original image by Hoyt & Taylor, 1977); (b) biopolymeric fluid threads generated from the cellular matrix upon cutting an okra in half (image courtesy J. Bico, unpublished); (c) ‘bag breakup’ of a droplet being atomized by a high-speed aerodynamic flow (reproduced from Romagnoli et al. 2000 [4]); (d) forward roll-coating of three aqueous solutions of hydroxyethyl cellulose (HEC) with increasing molecular weight from left to right (reproduced from Fernando et al., *Prog. Org. Coat* (2001) [5]; (e) formation of a beads on a string morphology on a nano-scale following electrospinning of an aqueous polyethylene oxide solution (Fong et al., *Polymer* 1999 [6]).

dispersion. Figure 1(d) depicts the formation of strands during a high-speed forward roll-coating operation (at 152 m/min) with aqueous solutions of hydroxyethylcellulose (HEC). The thickness, length and lifetime of these strands increases from left to right with the molecular weight of the HEC. Measurements show that the subsequent formation of a ‘roll-mist’ from breakup of these threads is directly connected to the extensional viscosity of the fluid [5].

Viscoelastic effects can also be important on the microscale, and high molecular weight additives contribute to the stability of electro-spinning processes [6]. As indicated in figure 1(e), complex morphologies can arise depending on the relative balances of capillarity (which leads to droplet formation) and fluid elasticity (which tends to lead to filament formation)

The phenomena shown in figure 1 are commonly described in heuristic and poorly-quantified adjectives such as ‘spinnability’, ‘tackiness’ and ‘stringiness’ [7]. Additional specialized terms are used in other industries including ‘pituity’ in lubricious aqueous coatings, ‘body’ and ‘length’ in printing ink business, ‘ropiness’ in yogurts and ‘long/short textures’ in starch processing. Other common examples encountered in every-day life include the spinning of ultra-thin filaments of silk by orb-weaving spiders, the stringiness of cheese, the drying of liquid adhesives, splatter-resistance of paints and the unexpectedly long life-time of strands of saliva.

In each case, the material property embodied in the formation and lifetime of a filament is some specific measure of the transient extensional stress growth function for the fluid of interest as a function of the strain imposed and the strain-rate resulting from capillary thinning. Visual descriptions of early experiments with plant cytoplasm represent some of the first investigations of fluid extensional viscosity (or *viscidty*) and are described by D’Arcy Thompson (1961). Petrie [8] summarizes the early literature in his monograph, and detailed reviews of experimental techniques for measuring both the transient and steady-state extensional stress growth for mobile fluid systems have been provided by Gupta & Sridhar [9] and James & Walters [10]. The fundamental governing equations for these free surface flows are derived in detail in the books by Yarin [11] and Middleman [12]. In the present article we focus on recent developments in understanding the fluid dynamics of the process of visco-elasto-capillary thinning and exploitation of such flows for extracting appropriate measures of the fluid’s resistance to stretching and breakup.

2. DEFINITIONS AND PARAMETERS

2.1 Background

In a pinching thread, viscous, inertial and elastic forces can all resist the effects of surface tension and control the ‘necking’ that develops during the pinch-off process. The dominant balance of forces depends on the relative magnitudes of each physical effect and can be rationalized by a careful dimensional analysis of the problem. The results can be conveniently represented in schematic form as shown in figure 2.

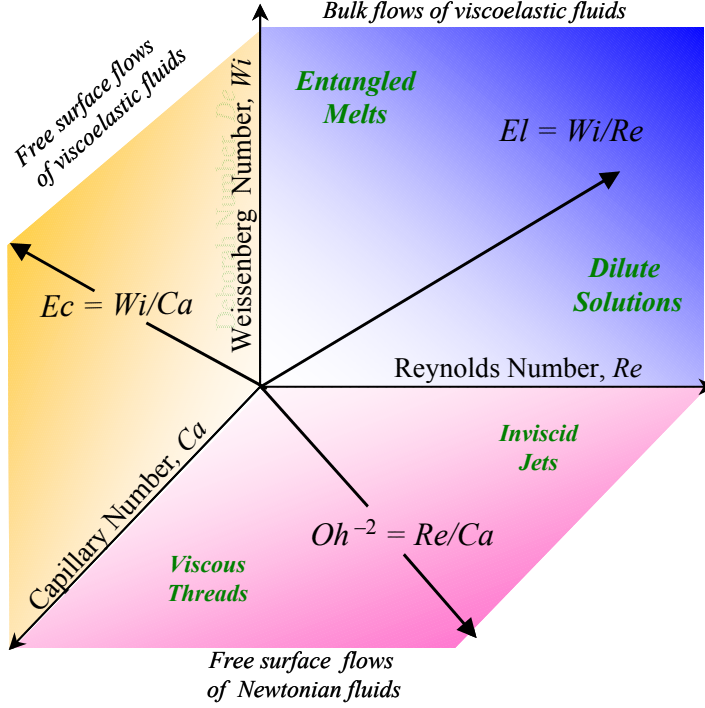


Figure 2: The operating space and important dimensionless parameters for Visco-Elasto-Capillary Thinning and Breakup.

For bulk flows of non-Newtonian fluids the relative importance of inertial effects and elastic effects with respect to viscous stresses are characterised by the Reynolds number, $Re = \rho V l / \eta_0$ and the Weissenberg number $Wi = \lambda V / l$, respectively. Here V and l are characteristic velocity and length scales for the flow of interest and ρ , η_0 , λ are the density, viscosity and longest relaxation time of the test fluid. Prototypical processing flows can be contrasted by their location in the back-plane of figure 2. The relative magnitudes of inertial stresses and elastic stresses can also be related by the elasticity number $El \equiv Wi / Re = \eta_0 \lambda / \rho l^2$, which is independent of the process kinematics and only depends on the fluid properties and the geometry of interest. For example, extrusion of polymer melts corresponds to $El \gg 1$, whereas processing flows for dilute polymer solutions (such as spin-casting) typically correspond to $El \ll 1$. Likewise free surface flows of Newtonian fluids can be characterised by the magnitude of the Reynolds number and the capillary number $Ca = \eta_0 V / \sigma$ (where σ is the surface tension of the fluid), and can be represented on the horizontal plane of the figure. The slope of trajectories in this plane is again independent of the imposed velocity and corresponds to the value of the Ohnesorge

number, $Oh^2 \equiv Ca/Re = \eta_0^2 / (\rho \sigma l)$, which may also be thought of as the inverse of a Reynolds number based on a characteristic ‘capillary velocity’ $V = \sigma/\eta_0$. Other combinations of these dimensionless parameters may also be used; for example, studies of high-speed jet breakup are commonly reported in terms of the Weber number $We \equiv ReCa = \rho V^2 l / \sigma$. The onset of the bag breakup regime shown in figure 1(c) then corresponds to the condition that the stagnation pressure at the nose of the droplet ($\sim \rho V^2 / 2$) exceeds the capillary pressure in the droplet ($\sim 2\sigma/R$); or equivalently to a Weber number (based on the droplet diameter) $We_D = \rho V^2 D / \sigma \geq 8$.

Inertialess flows of elastic fluids with a free surface are represented by the left-hand vertical plane, and the combined importance of elastic and capillary effects compared to viscous stresses is measured by another dimensionless parameter which can be referred to as an *elasto-capillary number*, $Ec \equiv Wi/Ca = \lambda \sigma / (\eta_0 l)$. Much less is known about flows in this plane. Bousfield et al. [13] were the first to study the nonlinear evolution of viscoelastic fluid jets and showed that increasing the elastocapillary number (denoted ϕ therein) resulted in strong stabilization of the jet. More recently, Spiegelberg and McKinley [14] and Rasmussen et al. [15] have investigated the effects of changes in Ec on adhesive fingering instabilities.

The three-dimensional interior of the parameter space shown in figure 2 corresponds to general visco-elasto-capillary flows. It is worth noting that as interest in microscale and nanoscale manufacturing intensifies, and the characteristic length scale (l) of a particular process decreases, the elasticity number and elastocapillary number will both increase. Non-Newtonian effects in the processing of complex fluids will thus become increasingly prevalent.

The relative co-ordinates of a particular process or geometry can be specified by values of $\{Re, Ca, Wi\}$. Since all three of these parameters vary with the characteristic process speed V , it is preferable to pick a single dynamical variable (say Re) and then specify the other coordinates using the material parameters, Oh and El . One final, particularly important, combination of parameters is the ratio $De_0 \equiv El/Oh = \lambda \sigma^{1/2} / (\rho l^3)^{1/2}$, which we define as a natural or *intrinsic Deborah number* for free surface viscoelastic flows since it represents the ratio of the time scale for elastic stress relaxation, λ , to the ‘Rayleigh time scale’ for inertio-capillary breakup of an inviscid jet, $t_R = (\rho l^3 / \sigma)^{1/2}$. Again it is worth noting that as length scales decrease non-Newtonian effects in free surface flows of complex fluids will become increasingly prevalent.

2.2 Prototypical Flow Configurations

There are many possible free surface conformations that may be realized during the thinning and break-up of complex liquids. In the present review, we focus on three specific geometries that have been studied extensively and systematically. These simple prototypical configurations are shown in figure 3 and they may be conveniently distinguished from each other by the relative magnitudes of the imposed velocity V and the natural or intrinsic speed of a capillary wave in the system of interest; in the

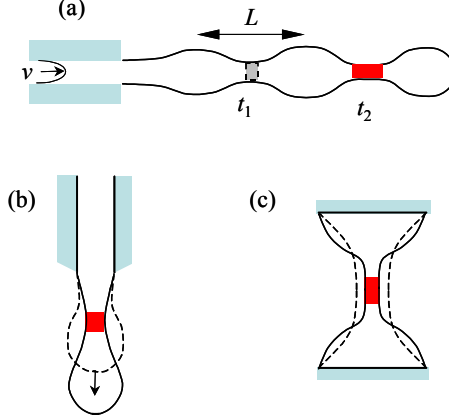


Figure 3: Three prototypical geometries for studying breakup of complex fluids; (a) continuous jetting instability; (b) dripping from a nozzle; (c) necking and breakup of a liquid bridge.

case of a low viscosity fluid ($Oh < 1$) this is given by $V_{cap} \sim (\sigma/\rho R)^{1/2}$, or alternately, for a viscous fluid thread ($Oh > 1$), the relevant scale is $V_{cap} \sim \sigma/\eta_0$.

The motion of a continuous jet of fluid shown in figure 3(a) exiting a circular nozzle of radius R_0 at a velocity $V \gg V_{cap}$, leads to a progressive necking and breakup as the jet flows downstream. In a dripping experiment of the type shown in figure 3(b) the exit velocity is of the same order as the capillary wave driving the breakup process ($V \sim V_{cap}$) and leads to the formation of a single hemispherical droplet at the exit of a small capillary tube of radius $R_0 \leq l_{cap} \sim (\sigma/\rho g)^{1/2}$, followed by gravitational drainage and capillary-induced pinch-off. Finally, in the liquid bridge configuration of figure 3(c), the imposed velocity is zero (following the initial rapid formation of a liquid bridge constrained between two concentric and axisymmetric endplates) and the bridge evolves purely under the action of viscous, inertial and capillary forces.

In each case the geometry is simple enough to be amenable to theoretical or numerical analysis of the time-evolving filament profile $R(z, t)$ and the flow can be controlled (at least initially until capillarity takes over) by motion of the end-plates or by controlling the supplied flow rate. Flows of Newtonian fluids in these geometries have recently been reviewed by Basaran [16]. The principal benefit of the third geometry is that the material element at the narrowest point or ‘neck’ (shown by the shaded elements in figure 3) remains located at approximately the same location in the laboratory reference frame; we denote the locus of this neck henceforth by $R_{mid}(t) \equiv R(z = 0.5L_0, t)$. The fixed Lagrangian location of the neck facilitates experimental measurement of the necking dynamics using either high-speed video-imaging or a laser micrometer system.

2.3 The Transient Extensional Viscosity

Although the dimensionless parameters discussed in §2.1 provide useful information for comparing different fluids and flow geometries, the Weissenberg number and Deborah number do not provide accurate measures of the effective elastic tensile stresses that can develop in a fluid thread which is necking down and elongating under the action of capillarity. Mathematically, such flows are ‘strong’ extensional flows which result in large molecular deformations of the underlying fluid microstructure [17]. The dominant flow in the slender fluid column is typically irrotational due to the absence of solid surfaces (which usually result in ‘no-slip’ boundary conditions and associated vorticity generation). For flexible polymer chains this deformation leads to large elastic stresses. If we consider an initially cylindrical fluid element of characteristic size $l = R_0$ then the strain rate is given by:

$$\dot{\varepsilon}(t) = -\frac{2}{R} \frac{dR(t)}{dt} = -2 \frac{d \ln(R(t)/R_0)}{dt}, \quad \dots\dots\dots(1)$$

and the total deformation of the fluid element after the thread has necked down to a size $R(t)$ is given by the logarithmic or Hencky strain [18]:

$$\varepsilon(t) = \int_0^t \dot{\varepsilon}(t') dt' = 2 \ln(R_0/R(t)). \quad \dots\dots\dots(2)$$

The actual stress in the filament can, in principle, be determined by numerical integration of a chosen viscoelastic constitutive equation with the known deformation profile $\dot{\varepsilon}(t)$. In many of the similarity solutions obtained for capillary thinning of slender fluid filaments (discussed in detail below in §4), the midpoint of the fluid filament is found to evolve according to a relationship of the functional form $R_{mid}(t) = C(t_0 - t)^m$ where C and m are parameters determined from the analysis. For example: for the Newtonian fluid $m = 1$; for a Second Order Fluid $m = 2$ and for a power-law fluid the parameter m is the power law exponent n . The strain rate and total Hencky strain of the fluid element at the mid-plane are then given by the expressions:

$$\dot{\varepsilon}_{mid}(t) = \frac{2m}{(t_c - t)} \quad \text{and} \quad \varepsilon(t) = 2 \ln \left(\frac{R_0}{C(t_c - t)^m} \right). \quad \dots\dots\dots(3)$$

It can be seen that both the fluid strain rate and the total strain therefore diverge as the breakup event approaches. It is thus possible to probe the extensional properties of complex fluids under conditions far from equilibrium and far beyond those attained in conventional torsional rheometers.

Following early disappointing attempts at correlating measurements of the extensional resistance of polymer solutions in different elongational devices (summarized in [10]), it is now recognized that the extensional viscosity of a viscoelastic fluid is best represented as a transient function of both the deformation rate (or Weissenberg number) and the elapsed time, or strain (see Ferguson et al for additional discussion).

To illustrate this, we consider for simplicity the particular case of the Oldroyd-B model [19] and a constant deformation rate ($\dot{\varepsilon}_0$). The radius of a fluid thread (in the

absence of surface tension) decreases according to $R_{mid}(t) = R_0 \exp(-\dot{\epsilon}_0 t/2)$. If the initial stress difference in the thread at time $t = 0$ is denoted $\Delta \tau_p^0 = (\tau_{p,zz}^0 - \tau_{p,rr}^0)$, then the evolution of the tensile stress difference can be found analytically and is given by:

$$\tau_{p,zz} = \left\{ \tau_{p,zz}^0 + \frac{G}{(1-0.5/Wi)} \right\} \exp(2\varepsilon(1-0.5/Wi)) + \frac{2\eta_p \dot{\epsilon}_0}{(1-2Wi)}, \quad \dots\dots\dots(4)$$

$$\tau_{p,rr} = \left\{ \tau_{p,rr}^0 + \frac{G}{(1+1/Wi)} \right\} \exp(-\varepsilon(1+1/Wi)) - \frac{\eta_p \dot{\epsilon}_0}{(1+Wi)}, \quad \dots\dots\dots(5)$$

where $G = \eta_p / \lambda$ is the elastic modulus, the Weissenberg number is $Wi = \lambda \dot{\epsilon}_0$ and the Hencky strain is $\varepsilon = \dot{\epsilon}_0 t$. After incorporating the additional Newtonian stress contribution from the solvents, the extensional stress growth function, or equivalently the *transient uniaxial extensional viscosity*, can then be represented in the form:

$$\eta_E^+(\dot{\epsilon}_0, t) \equiv \frac{(\tau_{zz} - \tau_{rr})}{\dot{\epsilon}_0} = 3\eta_s + \frac{(\tau_{p,zz} - \tau_{p,rr})}{\dot{\epsilon}_0}. \quad \dots\dots\dots(6)$$

Results are also often represented in dimensionless form as a transient Trouton ratio $Tr = \eta_E^+(\dot{\epsilon}_0, t) / \eta_0 \dot{\epsilon}_0$.

For small Weissenberg numbers ($Wi < 0.5$) the last terms in equations (4 - 5) dominate; however at $Wi = 0.5$, the coil-stretch transition leads to unbounded stress growth in time. It can be seen from equation (5) that the radial stresses typically decay with strain (ε) for all Wi ; however for Weissenberg numbers $Wi > 0.5$ the axial tension in a fluid filament grows without bound. It is this stress growth that results in the formation of fibrils and connecting ligaments observed in the images of figure 1.

Ultimately this stress growth is truncated by the finite extensibility of the molecules and can exceed viscous contributions to the stress by many orders of magnitude. This limit can be described by molecular models such as the FENE-P dumbbell model obtained from kinetic theory [20] and an additional finite extensibility parameter denoted L^2 herein. The axial stress growth is then truncated at a maximum value given by:

$$\tau_{p,zz, \max} = \eta_E \dot{\epsilon}_0 = 2\eta_p \dot{\epsilon}_0 L^2 (1 - 1/2Wi\dots). \quad \dots\dots\dots(7)$$

Finally, it can be seen from the expressions above that for $Wi < 0.5$ the effects of any initial stresses decay, *i.e.* the fluid exhibits a ‘fading memory’ as normally expected for a viscoelastic fluid; however, for $Wi \geq 0.5$, the initial axial stress does not decay but affects the flow at all future times. This is particularly important in the study of jet breakup – the effects of an upstream shear flow (for example in a pipe and nozzle) can significantly modify the dynamics of breakup. The role of pre-shear on extensional flow is not well understood yet and has only been considered by a handful of authors to date [21-23].

3. THE STABILITY OF FLUID JETS AND THREADS

Our understanding of visco-elasto-capillary thinning and break-up has advanced significantly over the past 10-15 years, through the combination of careful experimentation, numerical simulations of the governing equations and mathematical analysis of the stability of these equations. Some of the many papers in the area are collected in tabular form in table 1. This list is not intended to be exhaustive but rather highlights some of the key studies.

As we discussed above, the number of material parameters influencing the evolution of a fluid thread or jet can be rather large (cf. figure 2) and systematic studies have therefore focused on specific parts of this parameter space. In table 1 we indicate which contributions to the total force balance on the elongating thread considered in each study control the dynamical evolution and necking of the thread. In the present section we focus on experimental and theoretical studies of the linear stability of jets and liquid bridges (denoted by LS in table 1). In §4 we proceed to consider the nonlinear evolution of fluid threads through the use of self-similar solutions to the equations of motion, as well as through simpler but approximate ‘local’ analyses. These studies are denoted respectively by an SS and L in table 1.

3.1 Linear and Nonlinear Stability of Jets

It has been known since the 1960s that the evolution of viscoelastic fluid jets may be substantially different to common experience with Newtonian fluids. Linear stability analysis [33] shows that the jet is less stable to perturbations than the corresponding Newtonian viscous jet (because the fluid stresses that resist disturbance growth are always retarded behind the instantaneous deformation). For weakly elastic fluids this can result in jet breakup lengths that are shorter than those observed with a Newtonian fluid [39]. However, for highly elastic solutions containing high molecular weight additives, nonlinear effects can rapidly develop in the extensional flow that evolves in the neck region and stabilize the breakup process. This leads to significantly enhanced jet breakup lengths and the development of a *beads-on-a-string* morphology [1]. Bousfield et al. [13] simulated the viscoelastic extensional flow of a free jet using the Oldroyd-B model and showed that the elastic stresses grow exponentially in the neck as a result of the ‘squeezing’ flow induced by the ever-increasing capillary pressure $\sigma/R_{mid}(t)$. They also showed that the evolution in the filament profile can be accurately described by a simplified one-dimensional set of slender filament equations. This greatly simplifies the analytical and computational complexity of the task. The resulting one-dimensional equation set can also be conveniently represented in Lagrangian form [37] and a number of similarity solutions incorporating capillarity and viscoelasticity as well as additional effects of inertia and finite extensibility have been studied by Renardy [36]. The structure and development of the associated methodology is summarized in last year’s *Rheology Reviews 2004* [40] and discussed further in §4 below.

Author	Contribution to Filament Force Balance							Type	Remarks/Scaling
	C = capillary, V = viscous, I = inertia								
	E = Elastic, G = gravity, O = other.								
	C	V	I	E	G	O			
Keller & coworkers. (1983; 1990) [24, 25]	✓		✓				SS	$R \approx 0.64(\sigma/\rho R_0^3)^{1/3} (t_c - t)^{2/3}$.	
Eggers (1993) [26]	✓	✓	✓				SS	$R = 0.0304(\sigma/\eta_s)(t_c - t)$.	
Papageorgiou (1995) [27]	✓	✓					SS	$R = 0.0709(\sigma/\eta_s)(t_c - t)$.	
Brenner, Lister & Stone (1996) [28]	✓	✓	✓				SS	Countably infinite solutions.	
Lister & Stone (1998) [29]	✓	✓				✓	SS	Viscous effects of an external fluid. $R \sim (\sigma/\eta_s)(t_c - t)^{1/2}$	
Moseler et al. (2000) [30]	✓	✓				✓	SS	Thermal Fluctuations; $R \sim (t_c - t)^{1/2}$.	
Stokes et al. (2000) [31]		✓			✓		N	Length also diverges in finite time; $R \sim (\rho g L_0 R_0^2/3\eta_s)^{1/2} (t_c - t)^{1/2}$.	
Smolka et al. (2005) [32]		✓		✓	✓		N	UCM/Oldroyd-B model.	
Middleman (1965) [33]	✓	✓	✓	✓			LS	Linear Jeffreys Model.	
Bousfield et al. (1986) [13]	✓	✓	✓	✓			N	Oldroyd-B; $R \sim \exp(-t/3\lambda_1)$.	
Hinch & Entov (1997) [34]	✓	✓		✓			L	Spectrum of time constants.	
Chang et al. (1999) [35]	✓	✓		✓			LS, SS, N	Oldroyd-B Model.	
Renardy (1995; 2002) [36, 37]	✓	✓	✓	✓			SS	FENE-P, PTT, Giesekus (& Inertia).	
Tirtaatmadja et al. (2004) [38]	✓		✓	✓			L	FENE-P.	

Table 1: A summary of recent studies on the dynamics of thinning fluid filaments. Legend: SS, similarity solution; N, numerical simulations; LS, linear stability analysis; L, local analysis (i.e. 0 + 1 (space + time) dimensions).

An important result from numerical study of the necking process is the possibility of an *elasto-capillary balance* in the necking thread. The exponential decrease in the radius (and concomitant exponential increase in the capillary pressure in the cylindrical thread $p_{cap} \sim \sigma/R(t)$), results in a constant strain rate (from equation (1)) and correspondingly an exponential growth in the axial tensile elastic stress (from equation (4)). Detailed analysis shows that the filament radius evolves in the form:

$$\frac{R_{mid}(t)}{R_0} \approx \left(\frac{G}{\sigma/R_0} \right)^{1/3} \exp(-t/3\lambda) \Rightarrow \dot{\epsilon}_{mid} = -\frac{2}{R_{mid}} \frac{dR_{mid}}{dt} = \frac{2}{3\lambda} \quad \dots\dots\dots(8)$$

The necking process thus corresponds to a homogeneous elongational flow with $Wi = \lambda \dot{\epsilon}_{mid} = 2/3$. Schümmer and Tebel [41] used this principle to motivate construction of a free jet elongational rheometer.

The elasto-capillary balance and resulting exponential stress growth obtained with a quasilinear model such as the Upper-Convected Maxwell or Oldroyd models precludes the possibility of filament breakup [42]. Ultimately we expect two additional effects to modify the dynamics; (i) fluid inertia and (ii) finite extensibility of the dissolved macromolecules. The interplay of these effects governs the tendency of the elongating and thinning fluid thread to form satellite droplets. These smaller droplets are of great importance commercially as they affect the delivery of inks and fertilizers in spraying and inkjetting operations. Although the general principles controlling this process are now well known, a quantitative and predictive theory or analysis for viscoelastic fluids remains lacking at present.

Simulations [13] of the size of the primary and secondary droplets resulting from the breakup of a Newtonian fluid jet as a function of the dimensionless wavenumber $k = \pi R_0/L$ of the disturbance are in quantitative agreement with experimental data as shown in figure 4(a). As the wavenumber of the disturbance increases, the sizes of both the primary and secondary droplets decreases monotonically; however a secondary droplet is always observed.

For the case of a dripping nozzle, Ambravaneswaran et al. [43] used a 1D slender-body approximation similar to that in [13] to develop a complete operating diagram for the formation of satellite droplets in terms of the Weber number and Ohnesorge numbers. Figure 4(b) shows that by careful choice of the fluid viscosity (or Ohnesorge number) it is possible to optimize the range of dripping velocities (or Weber numbers) for which no secondary droplets are formed.

For polymeric jets there have been few quantitative comparisons of theory and experiment. Christanti & Walker [44, 45] recently studied the droplet size distribution and jet breakup length for a series of aqueous polyethylene oxide (PEO) solutions. The jet was periodically excited using a piezo transducer element and the corresponding evolution of the jet was captured using high-speed video as shown in figure 5. As the molecular weight of the PEO solute increases, and elastic stresses in the fluid become increasingly important, the jet breakup evolves from the classical Rayleigh mode (which leads to formation of a primary droplet together with small secondary droplets as shown in the top frame) towards the ‘beads on a string’

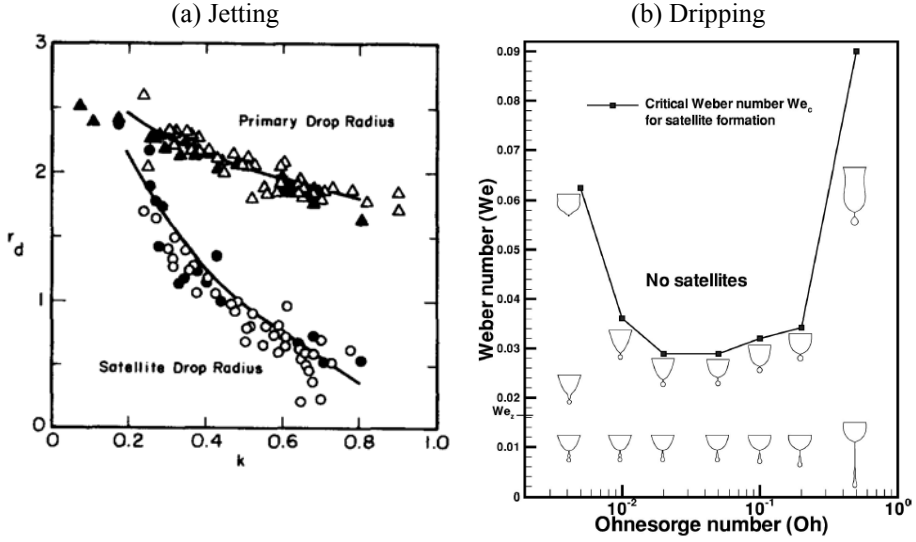


Figure 4: Formation of satellite drops during breakup of a Newtonian liquid thread; (a) Dimensionless droplet sizes (scaled with initial jet radius R_0) of the primary and secondary droplet size in breakup of a continuous Newtonian jet are shown as a function of dimensionless wavelength of disturbance, $k = \pi R_0 / L \sqrt{2}$. Reproduced from Bousfield *et al.* *JNNFM* 1986 [13]; (b) operability diagram showing the range of Weber numbers for which a satellite drop is/is not formed for different Ohnesorge numbers. Reproduced from Ambravaneswaran *et al.* *Phys Fluids* (2002) [43].

morphology shown in the lowermost frame. The wavenumber of the most unstable mode is clearly decreased with increasing fluid elasticity.

The authors also developed a phase diagram showing the range of fluid elasticities (as characterized by the longest or ‘Zimm’ relaxation time) and wavenumbers for which satellite droplets are eliminated (figure 5(b)). As the fluid elasticity increases, the range of wavenumbers for which the viscoelastic jet is able to suppress drop break grows rapidly. In dimensionless form, the elasticity of the polymer solutions is characterized by the intrinsic Deborah number De_0 defined in §2. For a fluid jet exiting a nozzle of radius 0.25mm, the fluid with measured relaxation time of 0.5 ms (0.1% 3×10^5 g/mol PEO) corresponds to a Deborah number $De_0 = 0.97$. For Deborah numbers below unity, elastic effects thus do not stabilize the jet and Newtonian-like breakup dynamics are observed. Very similar stabilization effects and suppression of satellite drops are also seen during the pinch-off of PEO solutions dripping from nozzles [46, 47].

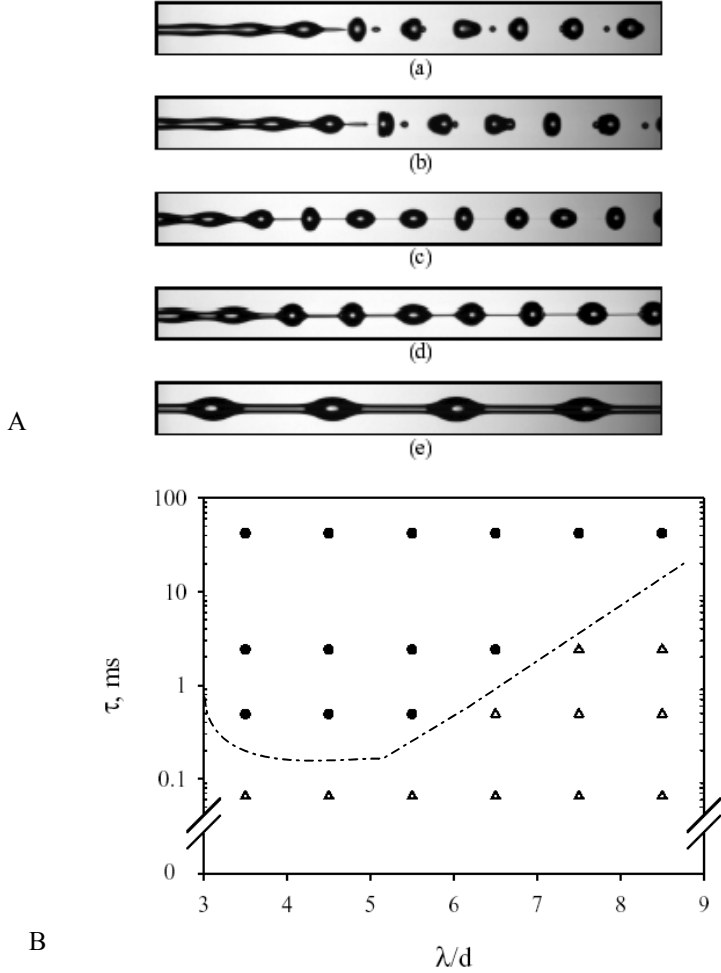


Figure 5: Effect of viscoelasticity on jet break up; (A) evolution in jet profiles due to a forced disturbance with wavelength $\lambda/d = 4.5$; (a) a Newtonian 50/50 water/glycerol mixture; (b) 0.3% 100kg/mol PEO; (c) 0.1% 300kg/mol PEO, (d) 0.05% 1000kg/mol PEO, and (e) 0.043% 5000kg/mol PEO. Flow direction is from left to right and the image size is 20 mm x 2 mm; (B) Stability diagram showing conditions which form satellites (Δ) and conditions which form no satellites (\bullet) as a function of fluid relaxation time and wavelength of disturbance. Reproduced from Christanti & Walker, *J. Rheol.*, 2002 [45].

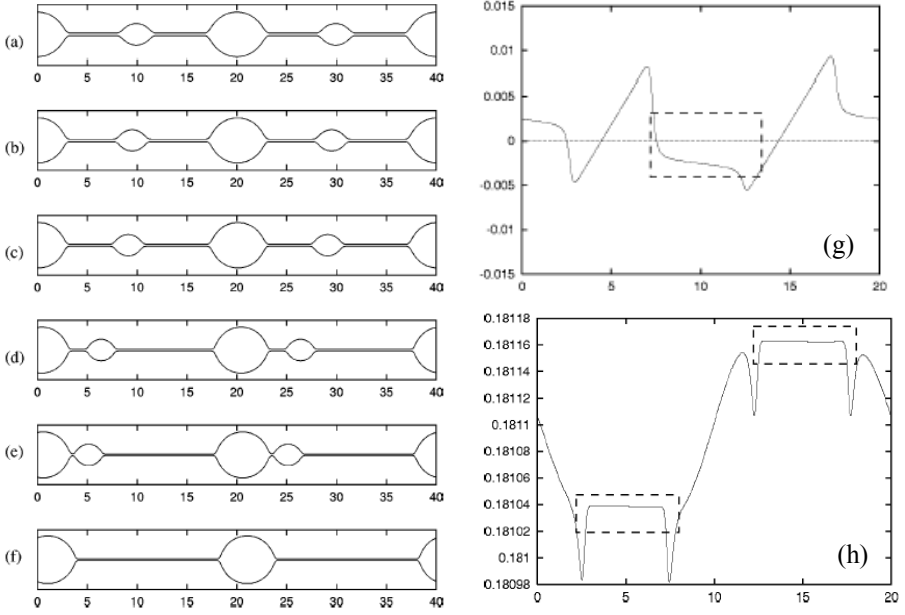


Figure 6: Numerical simulation of the formation and coalescence of beads on a string in an Oldroyd-B fluid; $De = 212.1$; $Oh = 1.41$; (a)-(f) filament profiles at dimensionless times (scaled with the Rayleigh time t_R) of $t = 56.6, 141.4, 212.1, 353.6, 381.8$ and 424.3 ; (g) axial velocity profile as a function of axial position (z/R_0); (h) dimensionless total axial force in the filament (scaled with surface tension σR_0) as a function of axial position. Reproduced from Li & Fontelos, *Phys. Fluids*, 2003 [48].

Recent advances in numerical methods that retain high resolution descriptions of the free surface can now enable the nonlinear dynamics of viscoelastic jets to be simulated very accurately as shown in figure 6. A small (1%) initial disturbance is supplied to the initial jet profile and the one-dimensional evolution equations for a slender Oldroyd-B filament are integrated forward in time [48]. The simulations show the growth of a large ‘primary’ drop and a smaller ‘secondary’ drop. Of particular interest are the velocity field and stress distribution in the filament, which are shown in figures 6(g) and 6(h). The velocity profiles show regions of homogeneous elongational flow in the threads (in which $v_z = \dot{\epsilon}_{mid} z$) interconnected by quasi-stagnant regions in the drops. A detailed analysis of the force balance in the thread shows that the net axial force is not identically zero as initially assumed in early theoretical analyses [34, 49] but in fact decays in time with the same exponential decay rate as the radius of the cylindrical regions. The contributions of capillary pressure and elastic stress in each

axial segment of the beads-on-a-string morphology are different and depend on the entire evolution history of the respective fluid elements. Consequently, small force imbalances and the slow drainage of fluid from the cylindrical threads into the interspersed droplets can result in a prolonged coalescence phase as shown in figure 6(a - f). Although the similarity between the experimental observations in figure 5 and numerical simulations is striking, a quantitative comparison between jet breakup/atomization experiments employing a well-characterized model polymer solution and numerical simulations with predetermined physical parameters has yet to be performed.

The simulations in figure 6 are appropriate for a dilute solution of infinitely extensible macromolecules (which can be modeled as Hookean dumbbells and described by the Oldroyd-B constitutive equations); however in a real fluid, at long times the finite extensibility of the molecules must become important. Renardy [36] and Fontelos & Li [50] have shown that in this limit a self-similar necking process (see §4) develops in which the radius no longer decays exponentially, but *linearly* in time with $R_{mid} \approx (\sigma/2\eta_E)(t_c - t)$ where η_E is the steady elongational viscosity and t_c is the critical time to breakup. Interestingly it is found [50] that the precise value of the numerical front factor in this relationship depends on details of the specific constitutive model, and this suggests that studies of elasto-capillary thinning and breakup might provide sensitive probes of the extensional rheology of complex fluids at large strains.

A recent theoretical stability analysis [35] has also shown that the elongated beads-on-a-string structure shown in the last frame of figure 6(a) may itself be unstable to a new mode of inertio-elasto-capillary instability. Numerical calculations showed that the neck region connecting the primary droplet to the elastically-dominated cylindrical ligament is unstable to small perturbations, leading to an elastic recoil and formation of a smaller secondary droplet connected to the main droplet by a finer-scale ligament. This structure is then itself unstable to perturbations and this process of ‘*iterated stretching*’ repeats indefinitely (for an infinitely extensible fluid model such as the Oldroyd-B model), with a well-defined recursion relationship between the size of each generation of beads. Iterated instabilities in fluid threads of very viscous Newtonian fluids ($Oh \geq 1$) have been observed previously [51], but due to the lack of a wavelength selection mechanism this instability does not lead to well-defined arrays of beads. Although hints of this iterated process have been noted in some careful photographs of polymeric threads [35, 45] an iterated elastic instability has yet to be observed definitively in experiments with polymer solutions. As noted by Chang et al. [35] fluid inertial effects are also important in this iterated process; in order to ensure that the growth rates of the beads (which scale with τ_R^{-1}) are faster than the thinning rate of the primary elastic thread (which is given by $(3\lambda)^{-1}$). A high molecular extensibility is also required in order to permit repeated stretching/recoil and multiple generations of droplets. Iterated stretching thus requires $Oh \ll 1$, $De_0 \geq 1$ and $L^2 \rightarrow \infty$ and is most likely to be observed in experiments with dilute solutions of very high molecular weight flexible polymers in a low viscosity solvent.

3.2 Static Stability of Liquid Bridges

In addition to the infinite jet, the liquid bridge configuration shown in figure 3(c) has become a common geometry for experimental studies of necking and break-up of elastic fluids. In such a configuration, the rigid end plates impose no-slip and no-flux boundary conditions in the radial and axial directions respectively. The latter is straightforward to impose through a constraint of fixed volume and/or constant length; however the former boundary condition can not be represented in a simple one-dimensional formulation of the type discussed in §3.1 [43]. Consequently studies have focused instead on the quasi-static stability of the liquid bridge; i.e. which configuration minimizes the interfacial energy of the fluid; a single deformed (typically non-cylindrical) column or two topologically-distinct fluid blobs with one attached to each end plate? Originally studied by Plateau [52], modern studies were reignited by the work of Gillette & Dyson [53]. The literature in the area is extensive because the geometry is relevant to the ‘float zone’ process in crystal growth and the perturbative effects of gravity limit the uniformity and size of the float zone (see Coriell [54] for further discussion) and the review of Meseguer et al. [55] for details of the present state of knowledge in the area.

The static stability boundary for a fluid droplet of volume V_0 bounded between two plates can be represented in the form shown in figure 7. The aspect ratio of the liquid bridge is $\Lambda = L/R_0$ and the dimensionless volume of the bridge (compared to the volume of a right-circular cylinder) is $\mathcal{V} = V_0/(\pi R_0^2 L_0)$. For $\mathcal{V} = 1$ the maximum statically-stable length of a fluid column is $\Lambda_{S,max} = 2\pi$ as first determined experimentally by Plateau [52] and theoretically by Rayleigh [56]. However for smaller or larger dimensionless volumes, the maximum length can be smaller or larger as shown in the figure. The stability boundary is comprised of three distinct segments (lines OD, DC, CO). The sketches of bridge shapes inset in the figure show the shape of the bridge at the loss of stability on each branch.

As noted in Gaudet et al. [57] thread break-up experiments typically start with a cylindrical configuration and the total physical volume is held constant as the bridge is elongated axially. In the quasi-static limit of very slow displacement, this corresponds to a sequence of equilibrium states (denoted by a subscript S) which follow a hyperbolic trajectory through figure 7 (shown by the dash-dotted line) given by $\mathcal{V}_S = \Lambda_0/\Lambda_S$. The bridge breaks when this hyperbola intersects the *minimum volume stability limit* (the lower right-hand part of the stability curve) shown in figure 7. This critical value will therefore depend on the initial aspect ratio (or equivalently the initial volume) of fluid column used. If we denote this functional relationship by $\Lambda_{S,break}(\mathcal{V}_0)$ then the Hencky strain at break is $\mathcal{E}_{S,break} = \ln(\Lambda_{S,break}/\Lambda_0)$. An interesting question that does not appear to have been addressed to date is what is the initial aspect ratio that maximizes this strain to break? Preliminary calculations suggest that it is a hyperbolic trajectory with $\Lambda_0^* \approx 0.16$, which intersects the minimum volume stability limit at $\Lambda_{S,break}^* \approx 0.57$ corresponding to a stretch of $\mathcal{E}_{S,break}^* = \ln(0.57/0.16) = 1.27$. This trajectory also achieves a tangency condition with the lower left-hand part of the stability curve.

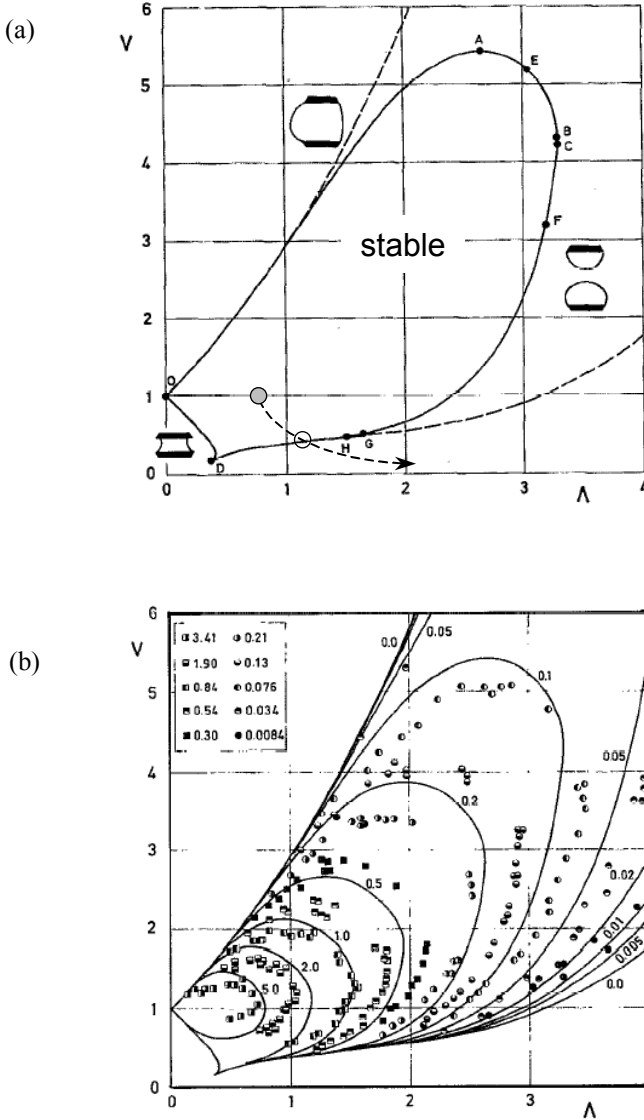


Figure 7: Stability diagrams for static liquid bridges confined between coaxial circular disks; (a) global stability diagram showing dimensionless volume V as a function of aspect ratio $\Lambda = L_0/2R_0$ for Bond numbers of $Bo = 0$ (---) and $Bo = 0.1$ (—). The bridge loses stability on the lower branch to a bifurcation into two identical ($Bo = 0$) or dissimilar size drops $Bo \neq 0$); On the upper branch the bridge loses axisymmetry; (b) Typical experimental data for Bond numbers $0 \leq Bo \leq 1$. Both figures reproduced from Slobozhanin et al. *Phys. Fluids* (1993) [58].

If there is a gravitational body force acting along the axis then this causes the bridge to ‘sag’ and also affects the stability boundary [58]. Because of its importance in silicon crystal growth, this effect has been considered in some detail. Gravitational effects are parameterized by the Bond number $Bo = \Delta\rho g R_0^2 / \sigma$ and even for $Bo = 0.1$, the domain of static stability decreases substantially as shown in figure 7(a). The resulting shape of the liquid bridge can be evaluated using a perturbation analysis for $Bo \ll 1$ [59, 60]. A bifurcation analysis can also be used [61] for small shape deviations and for small values of the Bond number to evaluate the shift in the stability locus and shows that the maximum aspect ratio for a given volume of fluid is:

$$A_{S,max} \cong 2\pi \left(1 - \left(\frac{3}{2}\right)^{4/3} Bo^{2/3} + \frac{1}{2}(\mathcal{V} - 1) \right) + \dots \quad \text{for } Bo \ll 1, \quad \dots\dots\dots(9)$$

However, for larger perturbations the solution must be found numerically. The results of a series of detailed theoretical calculations and microgravity experiments are shown in figure 7(b).

Most recent experimental studies of capillary thinning and breakup in polymer solutions utilize plates of radius $1 \leq R_0 \leq 6$ mm and fluids with surface tensions in the range $30 \leq \sigma \leq 70\sqrt{2}$ mN/m; Bond numbers are consequently of order 0.1 – 10. Axial distortions in the initial liquid bridge shape are thus expected to be quite pronounced. The axial extent of a liquid bridge can be extended by an external axial flow [62], a yield stress in the fluid [63] and also by bulk or surface viscoelastic stresses (cf. figure 8 in [64]). Of principal interest to the present review is the effect of dynamical stresses induced by axial stretching of the liquid bridge on the stability of the column. Experiments [65], stability analysis [66] and numerical calculations [57, 67, 68] show that this effect can be substantial. For a given value of the dimensionless volume \mathcal{V}_0 , the aspect ratio at break-up, or equivalently the total axial strain, $\varepsilon_p = \ln(L_{break}/L_0)$, appears to increase monotonically with capillary number beyond the quasi-static limit $\varepsilon_s(\mathcal{V}_0)$; however there is no simple analytic theory to describe this stabilization. This dynamic stabilization of a liquid bridge has recently been proposed as the basis for a ‘nano-rheometer’ [69].

If the imposed endplate deformation increases exponentially with time then measurement of the force exerted by the elongating liquid column on the endplate up to the point of break-up can be exploited to probe the transient extensional viscosity of the fluid. Preliminary experiments of this type were performed by Kröger & coworkers [65, 70] in a Plateau tank (containing a neutral-density fluid) and also in microgravity. Unfortunately inertial effects in the outer fluid and limitations in the duration of microgravity time prevented large strains from being achieved. By shrinking the size of the endplates (to minimize gravitational effects) and through careful selection of force transducers and radius measuring devices, such transient elongational measurements are now possible in the laboratory using *filament stretching extensional rheometers* without the need for reduced gravity environments (at least for fluids with viscosities greater than approximately $\eta_0 \geq 1$ Pa.s). Such instruments are beyond the scope of the present discussion but are reviewed in detail elsewhere [71].

4. DYNAMICS OF NECKING THREADS AND EVOLUTION TO BREAK-UP

In this section we focus on recent studies of the capillary-thinning and ultimate break-up of fluid threads far beyond the regime in which linear stability results are expected to be applicable. This field has been invigorated over the past fifteen years by the discovery of similarity solutions, which are valid for slender threads all the way to – and, in the case of viscous Newtonian fluids, even beyond – the singular point of break-up. Many of these developments are discussed in detail in the excellent review of Eggers [64] and the reader is referred there for mathematical details of the analyses for viscous and inviscid Newtonian fluids. Similarity solutions have also been discovered for the case of viscoelastic fluids, chiefly through the studies of Renardy [36, 37, 42] and have also recently been reviewed in *Rheology Reviews 2004* [40]. What is perhaps less clear is how this plethora of expressions are inter-related or how they may be exploited by the rheologist to measure material functions and we thus focus on these issues here. Similarity solutions to the one-dimensional radially-averaged form of the governing equations provide expressions for the velocity field and shape of the fluid thread which are valid not only for small perturbations to an cylindrical configuration but also for large disturbances that ultimately lead to a finite time singularity (at a time we denote generically t_c henceforth) and a topological bifurcation of the filament into two distinct regions. The interconnection between the numerous published similarity solutions can be represented in graphical form as shown in figure 8.

The relevant similarity solution for a particular experimental configuration depends on the relative magnitudes of the visco-capillary, inertio-capillary and viscoelastic time scales denoted $t_v = \eta_0 R_0 / \sigma$, $t_R = (\rho R_0^3 / \sigma)$ and λ respectively. The earliest studies of capillary-thinning for an inviscid thread or sheet [24, 25] (corresponding to potential flow (PF) with $Oh \ll 1$, $De_0 \ll 1$) show that close to breakup the minimum dimensionless thickness $h_{min} = R_{min}(t) / R_0$ decreases as the breakup event approaches with a power-law of the form $h_{min} \sim ((t_c - t) / t_R)^{2/3}$. Conversely, for a viscous Newtonian fluid ($Oh \gg 1$, $De_0 \ll 1$), the similarity solution obtained to the Stokes equation [27, 72] and analogous numerical simulations [73] show that the thread breaks linearly in time; and the midpoint radius decreases according to

$$h_{min} \equiv \frac{R_{min}(t)}{R_0} = 0.0709 \left(\frac{\sigma}{\eta_0 R_0} \right) (t_c - t) = 0.0709 Oh^{-1} \left(\frac{t_c - t}{t_R} \right). \quad \dots\dots\dots(10)$$

Later analysis has shown that this solution is only one of a countably infinite set; however all the other solutions are less stable to perturbations [28]. Eggers [26, 64] showed that there is another important ‘universal solution’ which incorporates viscous, inertial and capillary effects in the necking filament. We might expect this solution to be appropriate when the Ohnesorge number becomes $Oh \approx 1$; corresponding to length scales $l_E \sim \eta_0^2 / (\sigma \rho)$. When the expression for the thinning rate of the neck in this inertio-visco-capillary (IVC) solution is evaluated, it is found that it only differs from the visco - capillary (VC) expression (equation (10)) by a numerical coefficient (as indicated in figure 8) and the neck radius again decreases

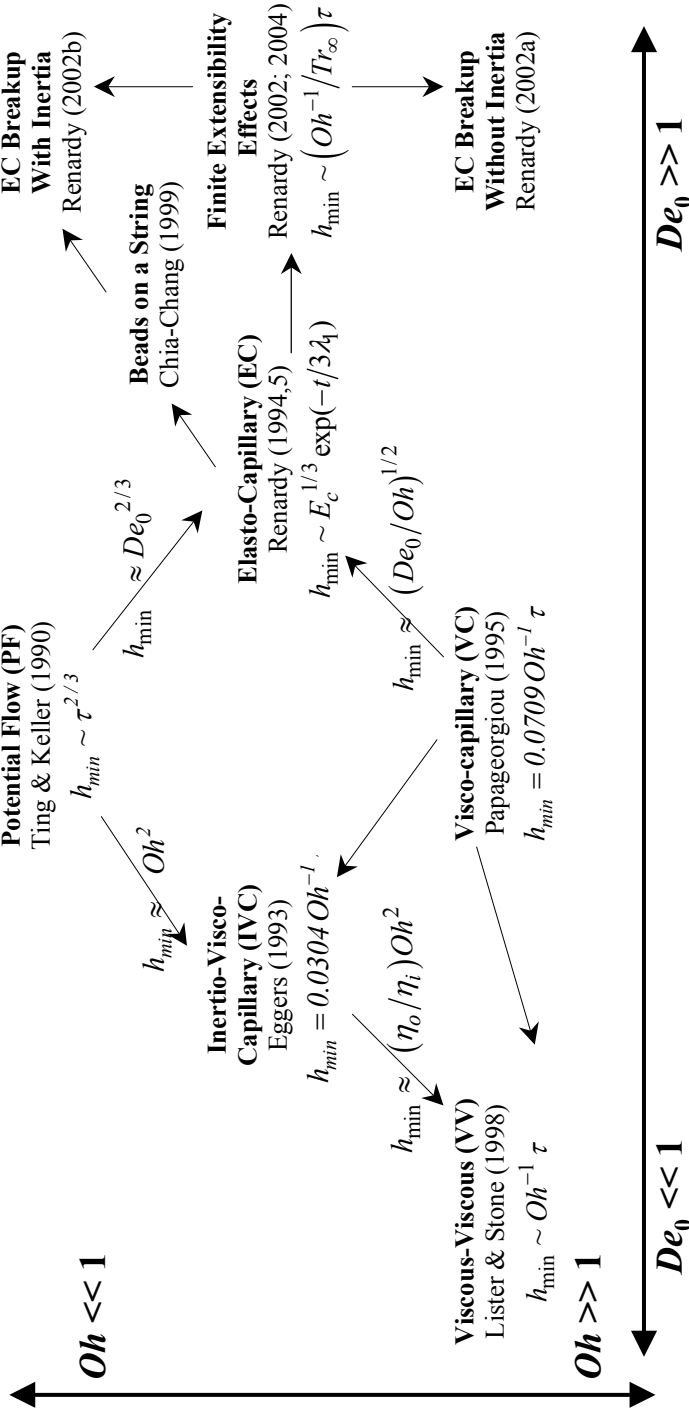


Figure 8: Inter-relationships between the different similarity solutions that have been discovered for self-similar filament thinning represented as a function of the intrinsic Deborah number $De_0 = \lambda/(\rho R_0^3/\sigma)^{1/2}$ and the Ohnesorge number $Oh = \eta_0/(\rho\sigma R_0)^{1/2}$. For each leading order balance, the dimensionless neck radius $h_{\min} = R_{\min}(t)/R_0$ is given as a function of dimensionless time $\tau = t/(\rho R_0^3/\sigma)^{1/2}$.

linearly in time (although it should be noted that in the IVC solution the location of the neck also translates slowly in the axial direction; whereas in the VC solution it is stationary). The fluid inertia does not appear in the expression for the necking rate because velocities are very small near the necking point. However at greater distances from the neck, the velocities become much larger and the IVC solution is strongly asymmetric, in contrast to the symmetric VC solution. Experiments and finite element simulations have shown the progressive cross-over from the inviscid PF solution to the IVC solution as viscous effects become important [74], and also from the symmetric VC to asymmetric IVC solution as the velocities in the neck diverge (according to equation (8)) and inertial effects become increasingly important [75, 76].

On very small length scales, additional forces become important and these have also been considered. It has been shown [29, 77] that ultimately viscous effects in the surrounding fluid become important (even if the outer fluid has a viscosity $\eta_0 \ll \eta_i$) and although the filament neck still decreases linearly with time, the shape of the filament in the neck region becomes conical and symmetric. If the viscosity of the outer phase is sufficiently large, analysis shows that the symmetric VC solution may crossover directly to this viscous-viscous balance without ever displaying the ‘universal’ IVC solution [29]. Interestingly, it has been noted very recently that in the case of an inviscid inner fluid core surrounded by a viscous fluid ($\eta_i \ll \eta_0$) that self-similarity breaks down because the necking rate in the inviscid thread is faster than the time scale required any for surface reconfiguration [78], and the thread never forgets the initial experimental conditions.

Recent experiments [79] have shown that similarity solutions to the governing equations of continuum mechanics are valid down to remarkably small length scales of $O(10 \text{ nm})$; however ultimately an additional length scale, corresponding to the wavelength of natural thermocapillary waves on the interface, $l_T \sim (k_B T / \sigma)^{1/2}$ (typically a few nm) becomes important. Beyond this point, the additional fluctuating stresses in the momentum balance must be considered [30] and these modify the necking so that the minimum radius varies with the square root of time from singularity.

When elastic effects become important, the dynamics of necking change significantly due to the additional elastic stresses that grow exponentially with the total strain in the fluid thread. For the Maxwell/Oldroyd-B model this leads to an exponential decrease in the thread radius as we discussed above in §3 for the case of viscoelastic fluid jets. The crossover to this elastic-capillary balance is to be expected when the viscoelastic time scale (λ) becomes of the same order as the visco-capillary or inertio-capillary time scale, and this crossover has been observed in both numerical simulations [13, 34, 49] and experiments [46, 47]. Ultimately, finite extensibility modifies this solution and the precise form of the corresponding similarity solution then depends on the relative importance of inertia and also on the precise form of the constitutive model [36, 50]. The additional constitutive parameters arising from viscoelastic constitutive models preclude a convenient representation on a two dimensional plot such as figure 8. Two important limits can be noted however;

(i) If the extensional viscosity approaches a constant value at large strain rates, then the corresponding tensile stress increases linearly with strain rate and the fluid acts like a highly anisotropic Newtonian fluid thread [34, 50]. As noted, in §3, the thread then necks linearly in time according to:

$$h_{\min} \approx (\sigma/2\eta_E)(t_c - t) = 0.5(Oh^{-1}/Tr_{\infty})\tau, \quad \dots\dots\dots(11)$$

where $Tr_{\infty} = \eta_E/\eta_0$ is the limiting value of the Trouton ratio at large strains and Weissenberg numbers. The precise value of the numerical front factor depends on the specific constitutive model [36, 50]. Large Trouton ratios dramatically retard the thinning compared to the equivalent Newtonian visco-capillary solution given by equation (10). For intermediate levels of extensional thickening, however, the filament may be *less* stable than the corresponding Newtonian fluid, because the elastic recoil and unloading of a stretched filament accelerates the local decay in the neck region [80]. In either case, the filament remains slender and the most unstable modes are long wavelength disturbances. Recent molecular dynamics simulations with bead-rod chains show a similar gradual thinning and cohesive failure [81].

(ii) Conversely, if the extensional stress is bounded at large strains (so that the elongational viscosity decreases) then the thread may fail purely through an elastic mechanism with capillarity playing no role [36, 40]. In this limit the usual energetic arguments that preclude short-wave length disturbances in the presence of capillary curvature terms are not relevant and so the possibility of elastic-like rupture events (of the kind reviewed in [82]) is to be expected. This has been observed in numerical simulations of filament thinning using the Papanastasiou-Scriven-Macosko (PSM) integral model [83]. Although qualitative observations of rupture events have been made in numerous elongated polymer samples, careful comparisons of numerical simulations with high-speed video imaging observations, or attempts at directly connecting the dynamics of rupture with the form of the tensile stresses in the underlying constitutive model, have yet to be considered.

5. CAPILLARY BREAK-UP EXTENSIONAL RHEOMETRY

The similarity solutions to the equations of motion discussed above show that the minimum radius of a fluid filament undergoing capillary-thinning (or ‘self-thinning’) evolves in a well-defined fashion with a distinctive dependence on time and a numerical front factor that contains material property information. This suggests that observation of visco-elasto-capillary thinning in slender filaments might provide a good basis for an extensional rheometer. This idea was first employed by Schümmer & Tebel [41] using a high-speed jet configuration; however Entov & coworkers [84-86] were the first to consider using the configuration of figure 2(c) in which a liquid bridge is stretched beyond its Plateau stability limit and then dynamically evolves under the action of capillary, viscous and/or elastic stresses.

In principle, the axial profile $R(z,t)$ of the evolving filament can be digitized and analyzed; however, close to break-up, the profile changes rapidly in the necked region and high-speed video may be required. It is more convenient to use a laser micrometer or other optical device to measure directly the midpoint radius $R_{mid}(t)$ of

the neck. Suitable non-contact laser profilometry instruments have been developed commercially for the wire-gauging and fiber-spinning industries; common manufacturers include Omron, Keyence, Zumbach and Mitutoyo. Typical devices may have a spatial resolution of 10 μm and sampling rates as fast as 10 kHz or more [87]. By monitoring the rate of necking and comparing the measurements with the appropriate theoretical model, one can then extract rheological parameters that characterize the transient extensional properties of the test fluid.

Experimental measurements always enable the determination of the critical time to break-up (t_c); and for many industrial operations (such as jet breakup, spray formation and atomization) this is the key parameter of interest. In addition, the measured evolution in the neck radius can also be converted into an *apparent extensional viscosity function* $\eta_{E, app}(\dot{\epsilon})$. Because the forces acting on the filament select a self-similar balance, the unknown viscous or viscoelastic stresses are in quasi-static equilibrium with the capillary pressure (provided fluid inertia is not important, so that $Oh \geq 1$). Using the definition in equation (1) we obtain

$$\eta_{E, app} = \frac{\Delta\tau}{\dot{\epsilon}_{mid}} = \frac{\sigma/R_{mid}(t)}{\dot{\epsilon}_{mid}} = \frac{\sigma}{-2 dR_{mid}(t)/dt} . \quad \dots\dots\dots(12)$$

In general, both the strain and the strain rate are changing as the thread necks and it is thus proper to refer to this as an *apparent extensional viscosity*. The material function defined in equation (12) is, however, the relevant one for studying and understanding commercial processes involving jet and thread breakup. It is also worth noting that in addition to serving as an extensional viscosity indexer, numerous recent studies have shown that a capillary thinning and breakup device can, under certain conditions, measure the true extensional viscosity. Just as in a conventional torsional rheometer, in order to extract values for specific material parameters it is necessary to select an appropriate constitutive model that can be regressed to the data. A diagnostic guide of the most commonly-observed modes of capillary thinning and break-up is shown in table 2, and the rest of this section focuses on a discussion of the different modes of thinning that can be observed.

5.1 The Force Balance on a Slender Filament

The expected form of the break-up profile can be obtained from a simplified one-dimensional form of the force balance on the thinning filament. In the limit of vanishing inertial effects, the governing equations can be integrated once to give a set of equations describing the forces acting on one-dimensional Lagrangian fluid ‘slices’. A detailed discussion of this approach and the connection with inherently one-dimensional Cosserat models is given in [64, 88]. A Lagrangian formulation of the governing equations for fiber-spinning in the absence of surface tension and subject to a constant axial force is discussed by Yarin [11]; however, the appropriate system of equations for capillary-driven breakup of a viscoelastic fluid thread with a time-varying tensile force was first discussed and analyzed by Renardy [37]. It has been shown that these one-dimensional equations can accurately reproduce full two-dimensional, time - dependent simulations with both the Newtonian and Giesekus

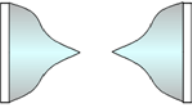
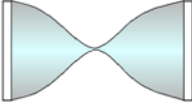
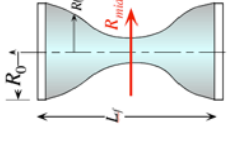
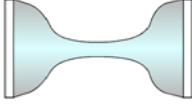
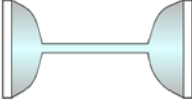
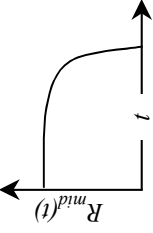
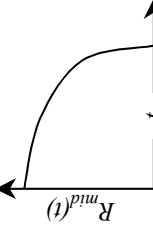
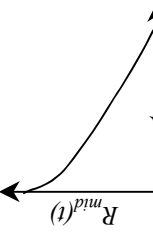
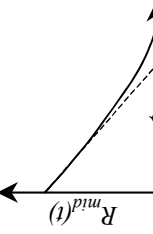
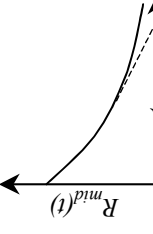
Bingham Plastic	Power Law Fluid	Newtonian	Weakly Elastic Fluid	Elastic Fluid
				
				
$\frac{R_{mid}(t)}{R_0} = \frac{\sigma/R_0}{\sqrt{3}\tau_y} \left[1 - \exp \left(-\frac{\tau_y(t-t_c)}{2\sqrt{3}\mu} \right) \right]$	$\frac{R_{mid}}{R_0} = \Phi(n) \frac{\sigma}{K} (t_c - t)^n$	$\frac{R_{mid}}{R_0} = 0.0709 \frac{\sigma}{\eta_s R_0} (t_c - t)$	$\frac{R_{mid}}{R_0} \approx \frac{\sigma}{48b_E R_0} (t_c - t)^2$	$\frac{R_{mid}}{R_0} = \left(\frac{GR_0}{2\sigma} \right)^{1/3} \exp(-t/(3\lambda_a))$
<p>Critical radius for yield and onset of capillary-driven flow is: $R < R_y = \sigma/\sqrt{3}\tau_y$</p> <p>Close to break-up, when viscous effects dominate, the radius decreases linearly in time.</p>	<p>The front factor Φ must be determined numerically (Doshi et al. 2003): $\Phi_{1D} \approx 2^{-n}/3$ $\Phi_{num} = 0.071 + 0.239(1-n) + 0.548(1-n)^2 + O(1-n)^3$</p>	<p>The front factor is determined from the similarity solution for Stokes flow (Papageorgiou, 1995): $t_c = 14.1 \eta_s R_0 / \sigma$</p>	<p>The Second-Order Fluid model gives: $\eta_E = 3\eta_0 + 3b_E \dot{\epsilon} + \dots$, where: $b_E = (-b_2 + b_{11}) > 0$ $t_c = \sqrt{48(b_{11} - b_2)/\sigma}$</p>	<p>Homogeneous extensional flow with $Wt = \lambda_a \dot{\epsilon} = 2/3$. Filament does not break without considering finite extensibility of polymer chain: $t_c \approx 3\lambda_a \ln \left[\frac{4}{3} L^2 (GR_0/\sigma)^{4/3} \right]$</p>

Table 2: A summary of the most commonly-observed modes of capillary thinning and break-up. The qualitative profile of the liquid bridge and the temporal evolution of the midpoint filament diameter for a number of constitutive models are shown.

constitutive equations [80]. As originally formulated, the equation derived by Renardy is written in terms of a Lagrangian *stretch* for each axial slice of the column defined as:

$$S(Z_0, t) \equiv \partial z / \partial Z_0 = R_0^2 / R(z(Z_0, t))^2, \quad \dots\dots\dots(13)$$

where $z(Z_0, t)$ denotes the Lagrangian position at time t of the one-dimensional fluid ‘slice’ located originally at axial position Z_0 at time t_0 . In experimental measurements of the midpoint radius or in digitized video images of liquid bridge shapes as a function of time, the radial profile $R(z(Z_0, t), t)$ is the primitive variable. If the stretch S is eliminated from the slender filament equation using equation (13) and the equation is extended to incorporate the effects of higher order axial curvature terms [64] and also an axial gravity field $\mathbf{g} = -g \delta_z$ we obtain the following stress balance:

$$\begin{aligned} \frac{F_z(t)}{\pi R^2} = & 3\eta_s \left\{ -\frac{2}{R} \left(\frac{\partial R}{\partial t} \right)_{Z_0} \right\} + [\tau_{p,zz} - \tau_{p,rr}] \\ & + \frac{\sigma}{R} \left\{ \frac{1}{[1 + (R')^2]^{1/2}} + \frac{R R''}{[1 + (R')^2]^{3/2}} \right\} - \frac{\rho g R_0^2 Z_0}{R^2}, \end{aligned} \quad \dots\dots\dots(14)$$

where $R = R(z, t)$ and the terms on the right-hand side represent, respectively, the net viscous extensional stress, the non-Newtonian tensile stress difference, capillary pressure arising from radial and axial curvature and gravity. This equation can then be combined with algebraic or differential equations for the axial and radial stress components that are obtained from a particular constitutive model. The resulting equation set can then be solved analytically or numerically. The net force in the filament is not zero but is independent of spatial position (i.e. the force along the filament is constant at any instant in time); it can thus be found by an integral constraint along the length of the evolving fluid column. Renardy [40] outlines a number of solutions that are valid in the limit that the last two terms capturing the higher order axial curvature and gravitational body force acting on the filament are negligible.

An even simpler *zero-dimensional* solution is possible if a further simplification is made: the fluid thread is approximated as an axially-uniform cylindrical column of constant radius $R_{mid}(t)$ which is necking down under the action of a capillary pressure $p_{cap} = \sigma / R_{mid}(t)$. The fluid ‘blobs’ at either end plate serve as quasi-static reservoirs which soak up the fluid drained into them from the necking region and also alleviate the no-slip boundary condition which would otherwise induce a radial shear flow near the ends of the radially-contracting fluid thread. The line tension acting at the junction of the cylindrical surface and spherical blob then results in an axial force $F_z(t) = 2\pi\sigma R_{mid}(t)$. Substituting these expressions into equation (14) and neglecting the asymmetric driving force of gravity results in an even simpler approximate stress balance of the form:

$$3\eta_s \left\{ -\frac{2}{R_{mid}(t)} \frac{dR_{mid}(t)}{dt} \right\} \approx \frac{\sigma}{R_{mid}(t)} - [\tau_{p,zz} - \tau_{p,rr}]. \quad \dots\dots\dots(15)$$

It can be seen from this expression that the capillary pressure $\sigma/R_{mid}(t)$ can be balanced by a viscous extensional stress $\sim 3\eta_s \dot{\epsilon}_{mid}(t)$ and/or by non-Newtonian contributions to the tensile stress difference in the column. It is this reduced *zero-dimensional* form of the force balance that is studied in most theoretical and experimental work [34, 87, 89] and is used in obtaining the different analytic expressions given in table 2.

In the first row of table 2, we indicate schematically the distinctive features and qualitative profile of the liquid bridge. In the second and third rows of the table, the expected temporal evolution of the midpoint filament diameter for a number of constitutive models are shown. It can be seen that the functional form of the necking profile can be very different and in each case is directly connected to the form of extensional viscosity predicted by a given constitutive model.

5.2 Elasto-Capillary Thinning of Dilute Polymer Solutions

Perhaps perversely, the elasto-capillary solution for a viscoelastic filament is easier to understand and validate experimentally than the corresponding expression for a viscous Newtonian fluid. This is because experiments (figure 5) and computations (figure 6) show that the approximation of an axially-uniform cylindrical thread is very good for a strongly-strain hardening fluid such as a dilute solution of a high molecular weight polymer. In this case the filament radius decays exponentially at a rate of $(3\lambda)^{-1}$ with a front factor that depends on the elastocapillary number (Ec). Physically, this corresponds to the radius at which we obtain a balance of the elastic modulus ($G = \eta_p / \lambda$) and the ‘squeezing’ effects of capillary pressure [34, 35].

A representative series of early experiments with a range of polymer solutions is shown in figure 9 [90]. In each case, regression to a single exponential yields a characteristic relaxation time $\lambda(c)$. As the concentration (c) of polymer increases, the elasto-capillary thinning process slows down as a consequence of the increase in the material relaxation time. At late times, two effects become evident; first a systematic deviation from exponential behavior, arising from finite extensibility; and secondly the discrete resolution of the laser micrometer can be seen in the ‘staircasing’ of the measured evolution in the filament diameter.

Entov & Hinch [34] also presented generalized expressions for elasto-capillary necking in a dilute solution of dumbbells with an arbitrary spectrum of relaxation times, $\lambda_i \{i=1, \dots, n\}$ and showed that after a short transitional period, the column selects a necking rate so that only the mode with the longest time constant is in fact being stretched. Anna & McKinley [87] considered the specific distribution of relaxation times expected for the Rouse-Zimm model $\lambda_i = \lambda / i^m$, with $m = 1.5$ or $m = 2$ corresponding to the Zimm model or Rouse model respectively. They note that because the longest mode achieves an elasto-capillary balance in which the Weissenberg number is $\lambda_1 \dot{\epsilon}_{mid} = 2/3$, all other modes experience a weak stretching flow

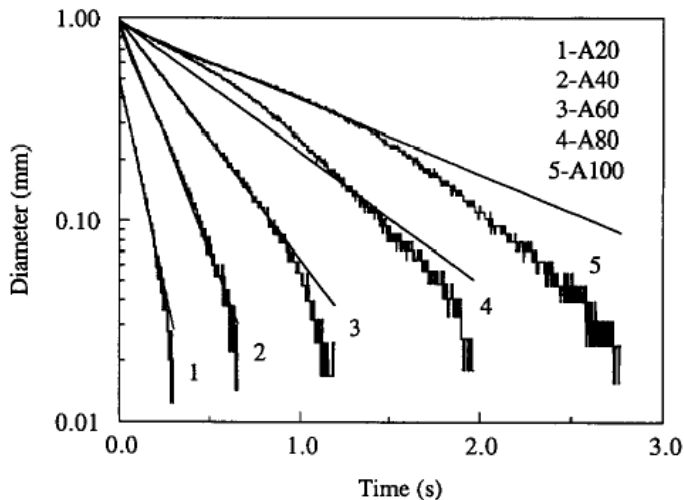


Figure 9: Elasto-capillary thinning for a series of semi-dilute polyisobutylene solutions dissolved in decalin. The average molecular weight of the PIB is 2×10^6 g/mol and the concentrations are 1% (A20), 2% (A40), 3% (A60), 4% (A80), 5% (A100) respectively. Reproduced from Liang & Mackley, *J. Non-Newt. Fluid Mech.* (1994) [90].

with $\lambda_i \dot{\epsilon}_{mid} = 2/3i^m$ which, for $i \geq 2$, is less than the critical value of 0.5 required for a coil-stretch transition in a uniaxial extensional flow. Because the stretching rate is constant in the exponential necking phase, the true transient uniaxial extensional viscosity is obtained; however, in contrast to a filament stretching device, it is not possible to vary the imposed deformation rate. Measurements for a series of polystyrene solutions with different high molecular weight solutes have shown the expected scaling in the longest relaxation time and quantitative agreement with linear viscoelastic measurements in small amplitude oscillatory shear flow [87]. An outstanding remaining challenge, however, is to understand the strong dependence of the experimentally-measured relaxation time on the polymer concentration even at concentrations well below c^* [38, 85].

5.3 Visco-Capillary Thinning of Newtonian Fluids

Dimensional analysis can be used to argue that – in the absence of inertia (i.e. so that $Oh \gg 1$) – a filament of Newtonian fluid (with viscosity $\eta_s \equiv \mu$) should neck down at a constant velocity $v_{cap} \sim \sigma/\eta_s$. If the surface tension is known from static tensiometry, then it should be possible to use measured variations in $R_{mid}(t)$ to find the viscosity of the fluid. Liang and Mackley [90] also performed experiments for a

Newtonian fluid but were unable to obtain agreement with independent measurements of the shear viscosity and surface tension. Similar problems were experienced in other early experiments with Newtonian fluids [89], and these findings limited the spread and utility of capillary thinning instruments. A comparison of the full axial profiles obtained from experimental capillary thinning experiments with a viscous oil and a dilute polymer solution is shown in figure 10. It is clear that for a Newtonian fluid, the approximation of an axially-uniform cylindrical filament is less appropriate.

Direct integration of the one-dimensional equation for a Newtonian fluid gives a linear variation in the filament profile with $R_{mid}(t) = (\sigma/(6\eta_s))(t_c - t)$ [34] and the numerical factor of $\sigma/6\eta_s R_0$ corresponds exactly to the growth rate of the fastest growing mode (of infinite wavelength) in Rayleigh breakup of a viscous fluid jet of radius R_0 [28, 64]. However this analysis is only applicable for infinitesimal perturbations about a cylindrical configuration and neglects the axial variations in the slenderness of the fluid thread and the long-range nature of viscous stresses in low Reynolds number flows. McKinley & Tripathi [91] used numerical calculations of the full one-dimensional governing equation (14) and experiments with Newtonian

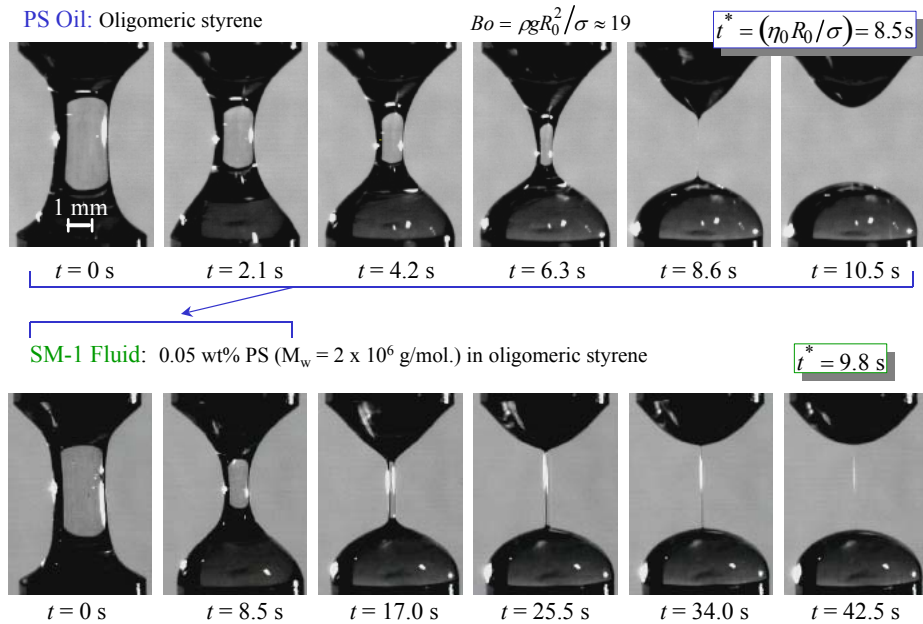


Figure 10: Comparison of temporal evolution in filament profiles for a viscous styrene oligomeric oil and the same oil containing 500ppm of a high molecular weight monodisperse polystyrene ($M = 2 \times 10^6 \text{ g/mol}$). Adapted from S.L. Anna, *PhD Thesis* 2000 [23].

calibration fluids to show that incorporating these axial variations as well as gravitational effects leads to additional contributions to the total force on the thread. At short times, gravitational sagging in the filament was found to be important (as can clearly be seen from the loss of top-bottom symmetry in figure 10) and leads to deviations from the similarity solution [91]. However, for sufficiently small radii so that gravitational effects are no longer important, the midpoint radius of a Newtonian fluid undergoing capillary thinning evolves according to the similarity solution of Papageorgiou [27] for visco-capillary (VC) necking indicated in figure 8 and table 2. In dimensional form this expression may be written:

$$R_{mid}(t) = 0.0709 \frac{\sigma}{\eta_s} (t_c - t) , \quad \text{for} \quad R_{mid} \leq \sqrt{\sigma/(\rho g)} . \quad \dots\dots\dots(16)$$

The critical time to breakup may be obtained by setting $R_{mid}(t = 0) = R_0$ to be $t_c = 14.1 \eta_s R_0 / \sigma$. The numerical front factor in this equation changes by a factor of more than 100% from the value of ‘6’ obtained from a simple zero-dimensional balance. Clearly, an accurate appreciation of this correction factor is critical if measurements of $R_{mid}(t)$ are to be used to extract quantitative values of fluid parameters that are consistent those measured in shear flows.

5.4 Elasto-Capillary Thinning revisited; the approach to full extension

Although the deviation is less marked, recent analysis has shown that there are also differences between the one-dimensional and zero-dimensional analyses for a viscoelastic fluid. The small, but non-zero axial gradients in the cylindrical thread lead to a net tensile force in the thread that scales with the thread radius $F_z(t) \sim R_{mid}(t)$ as expected but has a numerical coefficient that is slightly different from that assumed in the zero-dimensional analysis [48]. The self-similar nature of the necking process in a highly elastic fluid thread is shown in figure 11.

High resolution video-microscopy imaging and an edge-detection algorithm is used to image the junction region matching the cylindrical draining thread to the hemispherical quasi-static end-drop [92] as shown in figure 12(a). As time progresses this region becomes increasingly sharp. When plotted on a dimensionless scale normalized with the neck radius $R_{mid}(t)$ (here denoted $h_{min}(t)$) it is clear that the profiles progressively approach a single self-similar profile (figure 12(b)). These experimental observations are in good agreement with the similarity solution to the one-dimensional governing equation for the Oldroyd-B model shown by the dashed line in figure 12(b). This similarity solution predicts the same necking rate as the zero-dimensional elasto-capillary analysis (as given in equation (8)); however the front factor is modified by a factor of $2^{-1/3}$ as shown in table 2.

As we have noted in §4, when the molecules approach full stretch the necking dynamics cross-over from exponential to linear decay as given by equation (11) and indicated schematically by the dashed line in the rightmost figure of table 2. Entov & Hinch [34] use the FENE-P model to provide a very approximate estimate of the corresponding critical time to breakup.

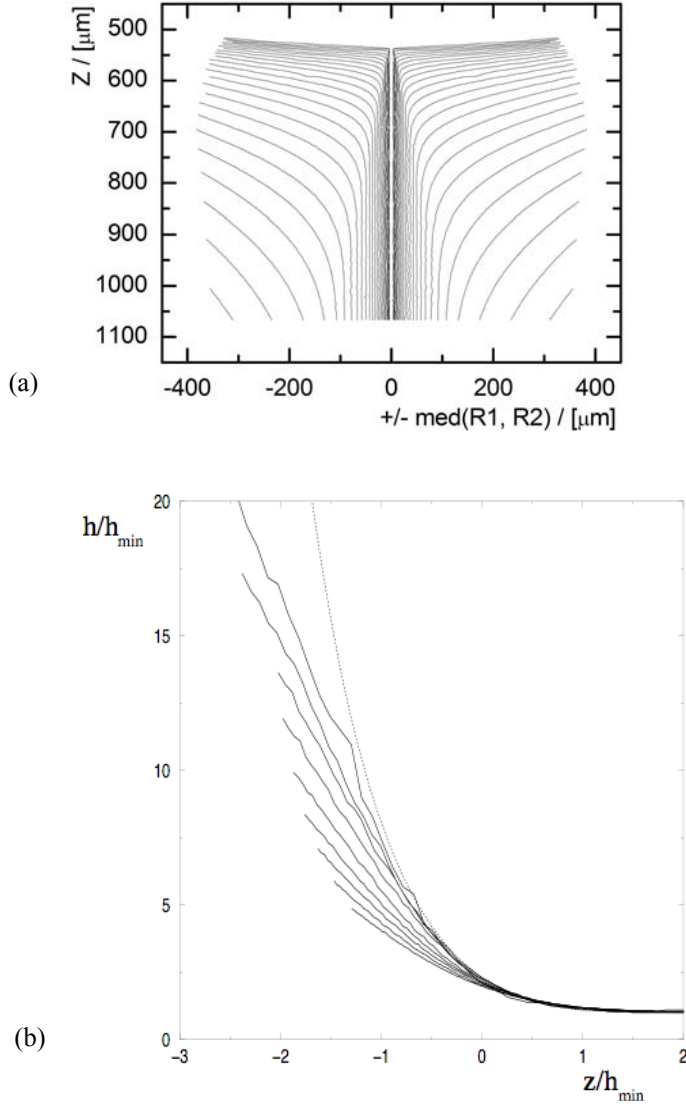


Figure 11: High resolution videomicroscopy showing the progressive formation of the corner region during capillary thinning in a PS/PS Boger fluid; (a) digitized filament profiles; each profile is separated in time by $\delta t = 2s \approx 0.4\lambda_z$; (b) the profiles slowly approach a self-similar shape when plotted in dimensionless form scaled with the minimum filament radius. Reproduced from Clasen et al. *J. Fluid Mech.* In press, (2005) [92].

Stelter et al. [93, 94] used careful measurements of the thinning dynamics in a wide range of different drag-reducing polymer solutions to construct nomograms of the measured relaxation time and the steady elongational viscosity; a representative example is shown in figure 12. The measurements show that the data lie along two distinct limiting curves; one for flexible non-ionic polymers (upper curve labeled ‘1’) and one for ionic polymers (labeled ‘2’) which exhibit aspects of rigid-rod like behavior as a result of charge repulsion along the chain.

This nomogram shows that as the relaxation time increases (either via increasing the molecular weight of the chain or the concentration in solution) the steady extensional viscosity also increases. The existence of two bounding curves provides a convenient method of rapidly assessing the molecular extensibility of a particular polymer chain. However the theoretical underpinnings of this empirical correlation have not been firmly established yet. Substitution of the analytic expression for the axial stress in a finitely-extensible dumbbell model given by equation (7) into the zero-dimensional force balance (equation (15)) confirms that observation of a linear radial decay in a capillary thinning experiment at long times indeed corresponds to measurement of the true terminal extensional viscosity: $\eta_{E,app} \rightarrow \eta_E = 3\eta_s + 2\eta_p L^2$. If the solvent contribution given by the first term in this expression is negligible then noting that the polymeric contribution to the viscosity is

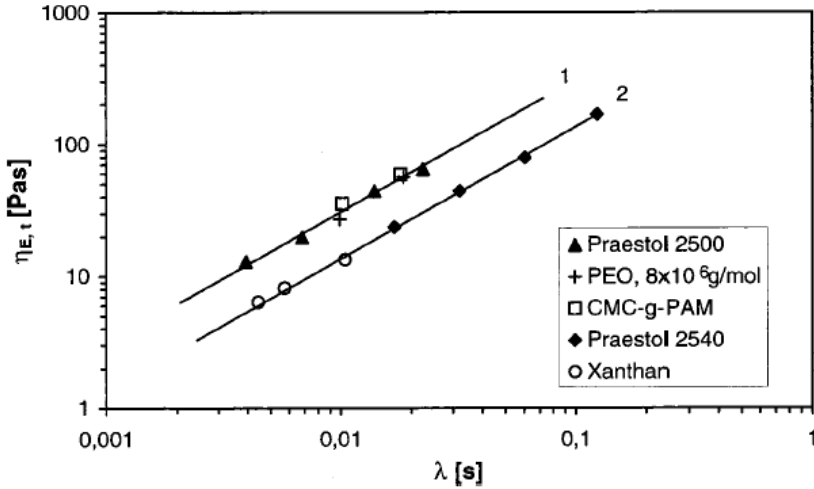


Figure 12: Variation of the steady-state apparent extensional viscosity (here denoted $\eta_{E,t}$) with the characteristic relaxation time (λ) for a number of aqueous solutions including polyacrylamide (‘Praestol’); polyethylene oxide (‘PEO’); carboxymethylcellulose (‘CMC’) and Xanthan gum. Curve ‘1’ denotes flexible coil behavior; curve ‘2’ denotes rigid rod behavior. Reproduced from Stelter et al. *J. Rheology* (2002) [93].

$\eta_p \equiv G\lambda = nk_BT\lambda$, we find that the steady elongational viscosity is linearly dependent on the relaxation time as shown in figure 12. However the molecular extensibility parameter is an independent parameter and so a family of curves is perhaps to be expected. The curves in figure 12 confirm the expectation that the molecular extensibility of an expanded ionic polymer is smaller than for a non-ionic flexible Gaussian chain. Stelter et al. [93] also show that as salt is progressively added to polyacrylamide solutions and the intramolecular charge repulsions are screened out, measurements of the η_E / λ relationship move laterally from curve ‘2’ to curve ‘1’; consistent with a decrease in relaxation time and an increase in molecular extensibility. Recent drop pinch-off experiments with polyelectrolyte solutions including partially-hydrolyzed polyacrylamide and DNA show that this increase in flexibility and the concomitant increase in the elongational viscosity correlate with enhanced turbulent drag reduction [95].

In general, molecular models such as the Rouse-Zimm model predict different scalings with molecular weight for the polymer relaxation time and for the steady-state extensional viscosity. The scaling of the former quantity with molecular weight is well known, $\lambda \sim M_w^{3\nu}$, where ν is the solvent quality exponent [96] and the scaling for the steady elongational viscosity can be found to be

$$\eta_E \approx G\lambda L^2 \sim \frac{cN_A k_B T}{M_w} (M_w^{3\nu})(M_w^{2(1-\nu)}) \sim M_w^{\nu+1}. \quad \dots\dots\dots(17)$$

In the limit of a theta solvent ($\nu = 1/2$) the scaling of relaxation time and elongational viscosity with M_w is identical, in agreement with the linear variation in the η_E / λ relationship observed in figure 12. For hydrodynamically-interacting chains in good solvents ($\nu \rightarrow 3/5$) there is a small difference in the scaling of the steady elongational viscosity ($M_w^{1.6}$) and the characteristic relaxation time ($M_w^{1.8}$). However large variations in the molecular weight would probably be needed to observe these effects in capillary thinning experiments and this may explain why no discernable spread in the data beyond a single line is seen in the experiments in [93]. Further considerations regarding the steady elongational viscosity of flexible and rigid polymers in solution are reviewed by James & Sridhar [97]. Repeated capillary breakup experiments on the same sample have also been used as a means to monitor the effects of extensional flow on the degradation of macromolecules commonly used in drag reduction studies [84, 89].

In most of the careful studies of capillary thinning in polymer solutions the fluids have been sufficiently viscous and elastic enough that gravitational drainage is relatively unimportant; however if the aspect ratio of the imposed stretching deformation is increased substantially then this can lead to pronounced asymmetries in the filament [98]. As the Ohnesorge number is decreased, inertial effects can also become important and careful control of the aspect ratio employed in experiments is critical. Rodd et al. [99] have recently presented a series of experiments with low viscosity aqueous solutions of polyethylene oxide in water and show that, in general, successful measurements of capillary thinning require either $De_0 \geq 1$ (for polymer solutions) or $Oh \geq 1$ (for Newtonian fluids).

5.5 Concentrated Polymer Solutions

As the concentration of polymer is increased, coil overlap and entanglement effects become increasingly important. Experimental measurements and constitutive models for such systems show that the steady extensional viscosity may show both extension-rate thickening and extensional-thinning depending on the imposed extension rate [100]. Consequently capillary thinning and breakup measurements may show pronounced deviations from the simple elasto-capillary balance appropriate for dilute solutions. This can be seen in the experimental measurements at the highest concentrations (A80, A100) in figure 9; the filament necking rate becomes increasingly rapid as the chains become increasingly deformed and disentangled. Capillary-thinning measurements on entangled polystyrene solutions show that the filament evolves on time-scales corresponding to the Rouse time for molecular stretching rather than on the longest (reptation) time scale [101]; however a quantitative theory for this evolution is presently lacking. Numerical calculations suggest that the Giesekus model provides a good qualitative description of entangled solution response in transient extensional flows [80, 102]; however, no simple analytic solution for the evolution in the midpoint radius is available for this, or any other nonlinear differential constitutive model.

Renardy uses asymptotic analysis [40] to show that for many nonlinear models the filament dynamics close to breakup change substantially and the radius can go to zero uniformly over a finite region of space rather than at a single point. This phenomenon has not been observed definitively yet but the consequences of entanglement effects in capillary thinning can be illustrated by the experimental images shown in figure 13. The fluid is a semi-dilute entangled solution of polystyrene in tri-cresyl phosphate (TCP) which has been well-characterized in both steady and oscillatory shear flows and is weakly strain-hardening in transient extensional flow [103]. As the filament necks, the formation of a thin elastic filament can be observed. However before the elasto-capillary similarity solution shown in figure 11 is fully established, the maximum elongational viscosity is reached, the necking rate in the central section increases and filament failure occurs. The enlargement of the final frame suggests that the ultimate breakup event occurs simultaneously at several spatial locations; however high speed and high resolution studies of breakup in entangled solutions are needed for definitive assessment.

5.6 Weakly Viscoelastic Fluids

In the limit of very weakly elastic liquids, elongated filaments and strands are not observed; however it can be seen from the form of equation (15) that *any* non-Newtonian contribution to the total stress may be expected to *retard* the rate of necking (as given by dR_{mid}/dt). Since the flow is elongational in character, the use of the Reiner-Rivlin class of models is appropriate to analyze the first effects of non-Newtonian stresses [19]. Following specification of the form of the two functions of the flow invariants in this model, the resulting equation set can then be integrated forward in time. For the simplest case of a second order fluid, the extensional viscosity can be expressed in the form $\eta_E = 3\eta_s + 3b_E\dot{\epsilon}$. This expression can be combined with

equations (1) & (15) and solved analytically. The resulting solution is implicit in time however, and is not given here. Instead we consider two appropriate asymptotic limits: for low deformation rates and short times, the material response is Newtonian and the necking rate is linear in time; however, close to breakup the quadratic term in the extensional viscosity expression dominates. In this regime, the filament radius decreases quadratically in time as indicated in the fourth column of table 2. The filament still breaks in finite time and both the strain and the strain-rate diverge, despite the extensional-thickening in the viscosity. Preliminary experiments in our lab using STP oil (a prototypical weakly elastic fluid employed by Joseph and coworkers in rod-climbing studies [104]) suggest that this is a simple but effective model for interpreting the first non-Newtonian effects in capillary thinning [105].

5.7 Generalized Newtonian Fluids

Renardy [36] has considered the case of Generalized Newtonian Fluids and shown that similarity solutions exist with an exponent that depends on the functional form of the viscosity and how it varies with deformation rate in the necking fluid thread. Recently Doshi et al. [106, 107] have considered the case of power-law fluids

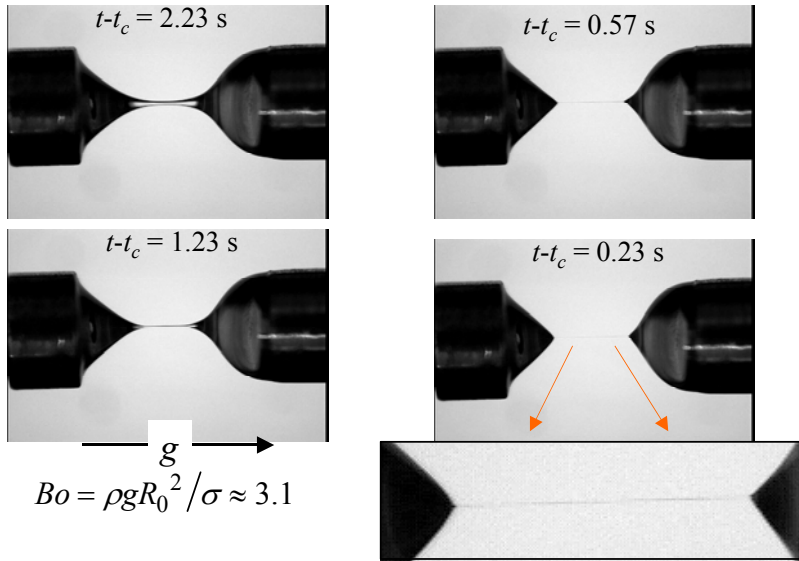


Figure 13: Images of the elastocapillary necking of a concentrated polystyrene solution (5wt% PS in tricresyl phosphate (TCP)). The shear rheology of the fluid is well described by a single Giesekus model with $\eta_0 = 59$ Pa.s, $\eta_s = 2$ Pa.s, $\lambda = 0.6$ s and $\alpha = 0.2$. Unpublished results; courtesy of O. Brauner and A. Tripathi.

and Carreau fluids in detail. In the region of the neck, the capillary pressure is high and consequently so is the necking rate. The local decrease in the effective viscosity in this region leads to a positive feedback effect and the necking rate accelerates continuously. The fluid column thus shows enhanced axial gradients and a ‘cusp-like’ profile close to the pinch region as indicated schematically in table 2. In fact a detailed analysis for the power-law fluid (both with and without inertia) shows that the slenderness assumption (i.e. that $dR/dz < 1$) is violated for a power law fluid with exponent $n \leq 2/3$ [107].

For a power-law fluid with constitutive equation $\tau = (K\dot{\gamma}^{n-1})\dot{\gamma}$, the midpoint radius varies as:

$$\frac{R_{mid}}{R_0} = \Phi(n) \frac{\sigma}{K} (t_c - t)^n, \quad \dots\dots\dots(18)$$

where n is the power-law exponent, K is the consistency index and $\Phi(n)$ is a numerical constant. A series of numerically-computed profiles are shown in figure 14(a).

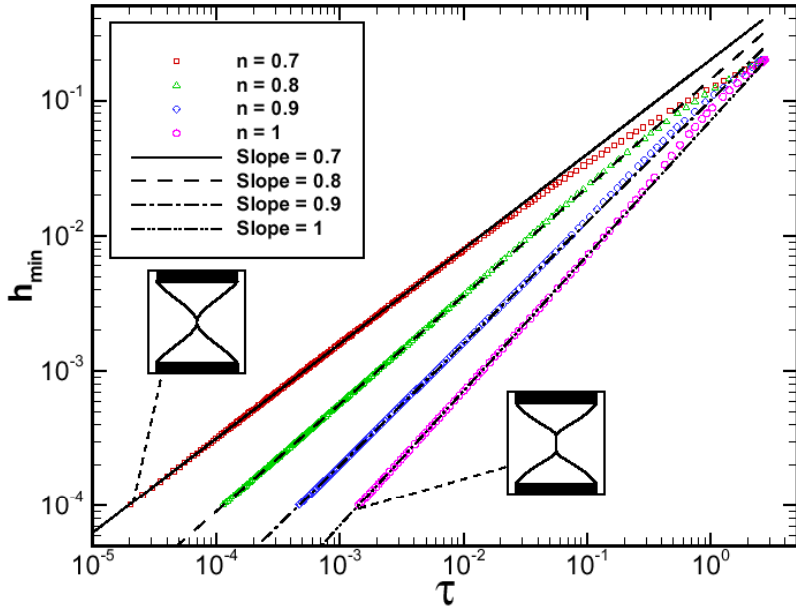
As the filament necks down and approaches the singular point of breakup (at $\tau = (t_c - t)/t_R = 0$) the midpoint radius is well-described by a power-law of slope n . Measurements with foods and consumer products which frequently exhibit inelastic shear-thinning behavior show that the rate of filament necking is well-approximated by this expression [108]. In figure 14(b) we show capillary thinning measurements in two yoghurt samples; one a whole-fat sample and the other a low-fat formulation. The image profiles (inset) from a high-speed video camera show the absence of a stringy appearance and instead reveal the development of a cusp-like region in the neck. Nonlinear regression of equation (18) to the data allows determination of the power-law exponent characterizing the fluid rheology (n) and also the time to failure (t_c) which is important in package-filling operations.

In general the front factor $\Phi(n)$ in equation (18) is a function of n and must be found numerically. The zero-dimensional model of equation (15) gives $\Phi_{1D} = 2^{-n}/3$ and a polynomial regression to the numerical solution of the full similarity equations [107] gives:

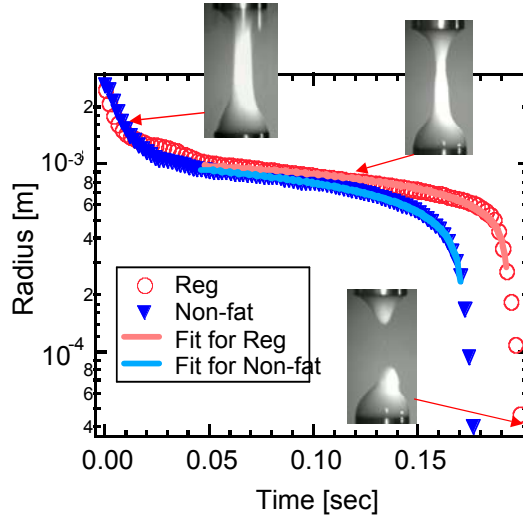
$$\Phi_{num} = 0.0709 + 0.2388(1-n) + 0.5479(1-n)^2 + 0.2848(1-n)^3 \quad \dots\dots\dots(19)$$

for $n \geq 0.6$.

In each of the above expressions, the correct Newtonian result is obtained for $n = 1$. In the case of a Carreau fluid, this power law-like necking is ultimately cut-off by the background Newtonian viscosity (η_∞) at very high deformation rates, and in this case the midpoint radius ultimately goes to zero linearly in time.



(a)



(b)

Figure 14: Two different representations of capillary thinning of a generalized Newtonian fluid: (a) evolution in the dimensionless radius $h_{min} = R_{mid}(t)/R_0$ as a function of dimensionless time from the singularity $\tau = \sigma(t_c - t)/\eta_0 R_0$. Reproduced from Doshi *et al.*, *J. Non-Newt. Fluid Mech.* (2003) [107]; (b) evolution in the (dimensional) radius as a function of time for two different yoghurt samples (a ‘non-fat’ and a ‘regular’ commercial yoghurt) together with a fit to equation (X); the images are obtained using a high-speed video camera. Reproduced from A.E.Park, *Msc Thesis* 2003 [108];

The case of a generalized Newtonian fluid with a yield stress is interesting but has not been studied in great detail to date. The single most important difference between a fluid exhibiting a yield stress and other fluids tested in capillary thinning and break-up devices is the existence of a critical sample radius (at the ‘neck’ or midpoint). The maximum capillary pressure in a thread of fluid is σ/R_{mid} and it is this that drives the fluid flow in the thread. If the yield stress exceeds this value, then capillary pressure is insufficient to generate a flow. The exact value for this critical radius has to be determined from the full solution to the problem; however, an *a priori* scaling estimate for the critical radius can be deduced on dimensional grounds to be given by $R_y \sim \sigma/\tau_y$. For sample radii $R > R_y$, then the thread or ‘liquid bridge’ will simply sit in static equilibrium and not evolve in time. This has been observed in careful experiments with liquid bridges of liquid crystalline materials which exhibit a yield stress [63]. Breakup of fluid jets with a yield stress have also been studied by Goldin et al. [109].

As the radius of a fluid thread decreases, the capillary pressure inside the fluid increases and will eventually exceed the value of the yield stress. This is why it is possible to observe stable liquid bridges of foods such as mayonnaise or ketchup connecting two solid surfaces (e.g. between one’s thumb and forefinger) when the thread radius is large, however these threads break when you pull your fingers apart – it is rare to see thin “stringy” threads of yield stress materials (unless high mol. weight additives are added). Solving the axially-uniform zero-dimensional equations gives the following expression for the midpoint radius

$$R_{mid}(t) = \frac{\sigma}{\sqrt{3}\tau_y} \left[1 - \exp\left(\frac{\tau_y(t-t_c)}{2\sqrt{3}\mu} \right) \right], \quad \dots\dots\dots(20)$$

with a critical radius $R_y = \sigma/\sqrt{3}\tau_y$. Validation of the accuracy of this equation has yet to be performed.

6. CONCLUSIONS AND FUTURE WORK

In this review we have surveyed recent experimental, numerical and theoretical advances in our understanding of the capillary-thinning and breakup of complex fluids. In addition we have attempted to note in each discussion some specific technical questions that remain outstanding. In this section we highlight more broadly some important areas for future research.

The liquid bridge geometry shown in figure 3(c) has become a standard laboratory configuration for studying visco-elasto-capillary thinning for the reasons highlighted above. However the other geometries are more relevant to commercial processing operations and additional computational and theoretical analysis of these configurations is needed. The addition of polymer to dripping jets and drop-on-demand inkjet printing configurations can inhibit breakup and completely eliminate satellite droplets [46, 47, 110].

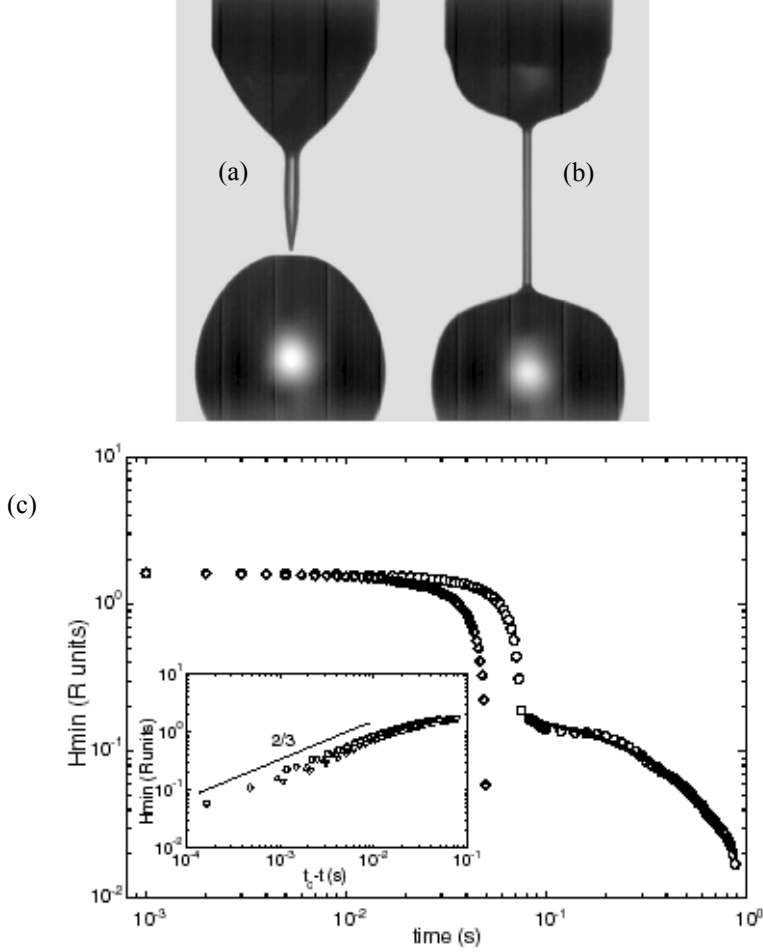


Figure 15: The effect of polymeric additive on drop pinchoff. (a) The image on left shows the pinch-off of a water droplet; (b) the inhibition of pinchoff through addition of 100ppm of PEO ($M \approx 4 \times 10^6$ g/mol). (c) The measured evolution in the neck radius initially shows rapid necking with $h_{min} \sim \tau^{2/3}$ before crossing over to a slower exponential decay at $t \approx 0.07$ s. Reproduced from Amarouchene et al., *Phys Rev. Lett.* (2001) [46].

An illustration of the dramatic effect of elasticity is shown in figure 15. The left-hand image shows the pinch-off of a droplet in a low viscosity Newtonian fluid ($Oh \ll 1$) and is now well-understood, both theoretically and numerically [43, 51, 64]. However the addition of high molecular weight polymer inhibits the singularity.

Measurements of the neck radius shown in figure 15(c) show that at short times the polymer does not modify the initial necking; however, there is an abrupt crossover from inviscid-like dynamics ($h \sim \tau^{2/3}$) to exponential elasto-capillary decay ($h \sim \exp(-t/3\lambda)$) as expected from figure 8. A simple zero-dimensional model of the neck evolution has recently been presented [38] but no numerical simulation of the complete one- or two-dimensional equations has yet been possible. Interestingly the system passes from an inertio-capillary to an elasto-capillary balance and viscous effects are thus irrelevant throughout. This suggests that studies of the dynamics of ‘inviscid elastic fluids’ (or more accurately ‘potential flows of viscoelastic fluids’) may be a viable avenue for future research. Joseph and coworkers have recently used such an approach to consider the linear stability of viscoelastic jets and find excellent agreement with the full linear theory [111, 112]; however, the extension to large amplitude deformations and nonlinear viscoelastic effects remains to be considered.

Other liquid bridge configurations have also been proposed as potential elongational rheometers for probing the response of complex fluids. In particular, the *filancemeter* has been developed as a method of probing the spinnability of viscoelastic biological fluids such as respiratory and cervical mucus [113, 114]. It has been known since the early work of Scott-Blair with bovine mucus that the apparent extensional rheology of these fluids varies significantly with hormonal cycles [115]. This has lead to patented devices that use ex-vivo measurements of the extensional viscoelasticity for probing fertility in both cows and humans [116]. The filancemeter uses an axial drive system to elongate a cylindrical liquid bridge linearly in time beyond its Plateau stability limit. The force in the stretched fluid column is not measured; however the variation in the total lifetime as the pulling velocity is varied can be determined with high accuracy by measuring the electrical conductivity between the upper and lower plates. Numerical calculations with Newtonian [68] and Generalized Newtonian Fluids [67] show that the length to breakup increases monotonically with the capillary number and also depends on the extensional rheology of the fluid. James has recently shown that measurements of the increased length to breakup resulting from non-Newtonian stresses can also be used to probe the extensional rheology of weakly elastic fluids such as printing inks and coating colors [117]. Careful experiments with Newtonian fluids suggest that the length to break increases beyond the Plateau stability limit with the square root of the separation velocity [118]; however, there is presently no analytic theory for Newtonian or non-Newtonian fluids.

Although we have reviewed experimental measurements for a large number of different materials in this article, the extensional rheology of several classes of complex fluids that have not been studied extensively to date; especially surfactant-based systems. Theoretical analysis of the necking of a viscous Newtonian thread in the presence of an insoluble surfactant shows that Marangoni stresses dramatically affect the necking dynamics and satellite formation; however ultimately the surfactant is convected out of the neck sufficiently fast that the visco-capillary solution of Papageorgiou is regained [119]. Linear stretching experiments with a soluble surfactant [120] show that, depending on the viscosity of the bridge, the presence of surfactant can either increase the length to breakup (if $Oh \gg 1$) or decrease it (if

$Oh \ll 1$). It will be interesting in the future to study other surfactant systems such as worm-like micellar solutions which exhibit strong strain-hardening in filament stretching experiments followed by sudden rupture events at high stresses [121].

7. ACKNOWLEDGEMENTS

I would like to acknowledge the stimulating discussions on this subject over a number of years with Oliver Harlen, Howard Stone, Vladimir Entov, Ole Hassager, Jens Eggers, Jie Li, Christian Clasen and Anubhav Tripathi. In addition I would like to acknowledge the assistance of the following people in my laboratory for providing me with unpublished results: A. Park, Dr. C. Clasen and Dr. J. Bico. Research on extensional rheology in my laboratory is supported by NASA, NSF and the Schlumberger Foundation and I gratefully acknowledge their support.

REFERENCES

1. Goldin M, Yerushalmi H, Pfeffer R and Shinnar R, "Breakup of a Laminar Capillary Jet of a Viscoelastic Fluid", *J. Fluid Mech.*, 38 (1969) 689-711.
2. Boger D V and Walters K, "Rheological Phenomena in Focus". Rheology Series, (Walters K, Editor), Elsevier, (1993).
3. Chen E B, Morales A J, Chen C-C, Donatelli A A, Bannister W W and Cummings B T, "Fluorescein and Poly(Ethylene Oxide) Hose Stream Additives for Improved Firefighting Effectiveness", *Fire Tech.*, 34 (1998) 291-307.
4. Romagnoli V, Felton P and Prud'homme R K. "Effect of Additives on Secondary Breakup of Droplets in High-Speed Airflows", Eighth Int. Conf. on Liquid Atomization and Spray Systems, Pasadena, CA (USA), (2000),
5. Fernando R H, Xing L-L and Glass J E, "Rheology Parameters Controlling Spray Atomization and Roll-Misting Behavior of Waterborne Coatings", *Prog. in Organic Coatings*, 42 (2001) 244-248.
6. Fong H, Chun I and Reneker D H, "Beaded Nanofibers Formed During Electrospinning", *Polymer*, 40 (1999) 4585-4592.
7. Jones W M and Rees L J, "The Stringiness of Dilute Polymer Solutions", *J. Non-Newtonian. Fluid Mech.*, 11 (1982) 257-268.
8. Petrie C J S, "Elongational Flows: Aspects of the Behavior of Model Elasticoviscous Fluids". *Research Notes in Mathematics*, Pitman (1979).
9. Gupta R K and Sridhar T E, "Elongational Rheometers", in *Rheological Measurement*, (Collyer A A and Clegg D W, Editors), Elsevier Applied Science, London, (1988) 211-245.

10. James D F and Walters K, "A Critical Appraisal of Available Methods for the Measurement of Extensional Properties of Mobile Systems", in *Techniques in Rheological Measurement*, (Collyer A A, Editor), Elsevier, London, (1993) 33-53.
11. Yarin A L, "Free Liquid Jets and Films: Hydrodynamics & Rheology". Interaction of Mechanics and Mathematics Series, Longman, Wiley, (1993).
12. Middleman S, "Modeling Axisymmetric Flows", Academic Press, (1995).
13. Bousfield D W, Keunings R, Marrucci G and Denn M M, "Nonlinear Analysis of the Surface-Tension Driven Breakup of Viscoelastic Fluid Filaments", *J. Non-Newtonian Fluid Mech.*, 21 (1986) 79-97.
14. Spiegelberg S H and McKinley G H, "Stress Relaxation and Elastic Decohesion of Viscoelastic Polymer Solutions in Extensional Flow", *J. Non-Newtonian Fluid Mech.*, 67 (1996) 49-76.
15. Rasmussen H K and Hassager O, "The Role of Surface Tension on the Elastic Decohesion of Polymeric Filaments", *J. Rheol.*, 45 (2001) 527-537.
16. Basaran O, "Small-Scale Free Surface Flows with Breakup: Drop Formation and Emerging Applications", *A.I.Ch.E. J.*, 48 (2002) 1842-1848.
17. Petrie C J S, "Extensional Flow - A Mathematical Perspective", *Rheol. Acta*, 34 (1995) 12-26.
18. Tanner R and Tanner E, "Heinrich Hencky: A Rheological Pioneer", *Rheol. Acta*, 42 (2003) 93-101.
19. Bird R B, Armstrong R C and Hassager O, "Dynamics of Polymeric Liquids. Volume 1: Fluid Mechanics", 2nd ed, Wiley Interscience, (1987).
20. Bird R B, "Polymer Kinetic Theories and Elongational Flows", *Chem. Eng. Commun.*, 16 (1982) 175-187.
21. James D F, McLean B D and Saringer J H, "Presheared Extensional Flow of Dilute Polymer Solutions", *J. Rheol.*, 31 (1987) 453-481.
22. Mena B, "A New Shear-Elongational Rheometer", in *Theoretical and Applied Rheology*, (Moldenaers P and Keunings, R, Editors), Elsevier, Brussels, (1992) 917-919.
23. Anna S L, "Filament Stretching Rheometry of Model Elastic Solutions", Ph.D. Thesis, Harvard University, Cambridge, MA (USA), (2000)
24. Keller J B and Miksis M J, "Surface-Tension Driven Flows", *SIAM J. Appl. Math.*, 43 (1983) 268-279.
25. Ting L and Keller J B, "Slender Jets and Thin Sheets with Surface Tension", *SIAM J. Appl. Math.*, 50 (1990) 1533-1546.
26. Eggers J, "Universal Pinching of 3D Axisymmetric Free-Surface Flow", *Phys. Rev. Lett.*, 71 (1993) 3458-3590.

27. Papageorgiou D T, "On the Breakup of Viscous Liquid Threads", Phys. Fluids, 7 (1995) 1529-1544.
28. Brenner M P, Lister J R and Stone H A, "Pinching Threads, Singularities and the Number 0.0304..." Phys. Fluids, 8 (1996) 2827-2836.
29. Lister J R and Stone H A, "Capillary Breakup of a Viscous Thread Surrounded by another Viscous Fluid", Phys. Fluids, 10 (1998) 2758-2764.
30. Moseler M and Landman U, "Formation, Stability and Breakup of Nanojets", Science, 289 (2000) 1165-1169.
31. Stokes Y M, Tuck E O and Schwartz L W, "Extensional Fall of a Very Viscous Drop", Q Jl. Mech Appl. Math, 53 (2000) 565-582.
32. Smolka L B, Belmonte A, Henderson D M and Witelski T P, "Exact Solution for the Extensional Flow of a Viscoelastic Filament", Eur. J. Appl. Math, (2005) in press.
33. Middleman S, "Stability of a Viscoelastic Jet", Chem. Eng. Sci., 20 (1965) 1037-1040.
34. Entov V M and Hinch E J, "Effect of a Spectrum of Relaxation Times on the Capillary Thinning of a Filament of Elastic Liquid", J. Non-Newtonian Fluid Mech., 72 (1997) 31-54.
35. Chang H-C and Demekhin E A, "Iterated Stretching of Viscoelastic Jets", Phys. Fluids, 11 (1999) 1717-1737.
36. Renardy M, "Similarity Solutions For Jet Breakup for Various Models of Viscoelastic Fluids", J. Non-Newtonian Fluid Mech., 104 (2002) 65-74.
37. Renardy M, "A Numerical Study of the Asymptotic Evolution and Breakup of Newtonian and Viscoelastic Jets", J. Non-Newtonian Fluid Mech., 59 (1995) 267-282.
38. Tirtaatmadja V, McKinley G H and Cooper-White J J, "Drop Formation and Breakup of Low Viscosity Elastic Fluids: Effects of Concentration and Molecular Weight", Phys. Fluids, (2004) submitted.
39. Mun R P, Byars J A and Boger D V, "The Effects of Polymer Concentration and Molecular Weight on the Breakup of Laminar Capillary Jets", J. Non-Newtonian Fluid Mech., 74 (1998) 285-297.
40. Renardy M, "Self-Similar Breakup of Non-Newtonian Fluid Jets", in *Rheology Reviews*, (D.M.Binding and K.Walters, Editors), The British Society of Rheology, Aberystwyth, (2004) 171-196,
41. Schümmer P and Tebel K H, "A New Elongational Rheometer for Polymer Solutions", J. Non-Newtonian Fluid Mech., 12 (1983) 331-347.
42. Renardy M, "Some Comments on the Surface-Tension Driven Breakup (or the lack of it) of Viscoelastic Jets", J. Non-Newtonian Fluid Mech., 51 (1994) 97-107.

43. Ambravaneswaran B, Wilkes E D and Basaran O A, "Drop formation from a capillary tube: Comparison of one-dimensional and two-dimensional analyses and occurrence of satellite drops", *Phys. Fluids*, 14 (2002) 2606-2621.
44. Christanti Y and Walker L, "Surface tension driven jet break up of strain-hardening polymer solutions", *J. Non-Newtonian Fluid Mech.*, 100 (2001) 9-26.
45. Christanti Y M and Walker L, "Effect of Fluid Relaxation Time on Jet Breakup due to a Forced Disturbance of Polymer Solutions", *J. Rheol.*, 46 (2002) 733-748.
46. Amarouchene Y, Bonn D, Meunier J and Kellay H, "Inhibition of the Finite Time Singularity during Droplet Fission of a Polymeric Fluid", *Phys. Rev. Lett.*, 86 (2001) 3558-2562.
47. Cooper-White J J, Fagan J E, Tirtaatmadja V, Lester D R and Boger D V, "Drop Formation Dynamics of Constant Low Viscosity Elastic Fluids", *J. Non-Newtonian Fluid Mech.*, 106 (2002) 29-59.
48. Li J and Fontelos M A, "Drop Dynamics on the Beads-on-String Structure for Viscoelastic Jets: A Numerical Study", *Phys. Fluids*, 15 (2003) 922-937.
49. Yarin A L and Entov V M, "Influence of Elastic Stresses on the Capillary Breakup of Dilute Polymer Solutions", *Fluid Dyn.*, 19 (1984) 21-29.
50. Fontelos M A and Li J, "On the Evolution and Rupture of Filaments in Giesekus and FENE models", *J. Non-Newtonian Fluid Mech.*, 118 (2004) 1-16.
51. Brenner M P, Shi X D and Nagel S R, "Iterated Instabilities During Droplet Fission", *Phys. Rev. Lett.*, 73 (1994) 3391-3394.
52. Plateau J A F, "Experimental and Theoretical Researches on the Figures of Equilibrium of a Liquid Mass Withdrawn from the Action of Gravity", in *Ann Rep. Smithsonian Institution*, (1863), 207-285.
53. Gillette R D and Dyson D C, "Stability of Fluid Interfaces of Revolution Between Equal Solid Circular Plates", *Chem. Eng. J.*, 2 (1971) 44-54.
54. Coriell S R, Hardy S C and Cordes M R, "Stability of Liquid Zones", *J. Coll. Int. Sci.*, 60 (1977) 126-136.
55. Meseguer J, Slobozhanin L A and Perales J M, "A Review of the Stability of Liquid Bridges", *Microgravity Sciences: Results and Analysis of Recent Spaceflights: Advances in Space Research*, 16 (1995) 5-14.
56. Rayleigh L, "On the Instability of Jets", *Proc. Lond. Math. Soc.*, 10 (1879) 4-13.
57. Gaudet S, McKinley G H and Stone H A, "Extensional Deformation of Newtonian Liquid Bridges", *Phys. Fluids*, 8 (1996) 2568-2579.
58. Slobozhanin L A and Perales J M, "Stability of Liquid Bridges between Equal Disks in an Axial Gravity Field", *Phys. Fluids A*, 5 (1993) 1305-1314.

59. Perales J M, Meseguer J and Martínez I, "Minimum Volume Stability Limits for Axisymmetric Liquid Bridges Subject to Steady Axial Acceleration", *J. Cryst. Growth*, 110 (1991) 855-861.
60. Szabo P, "Transient Filament Stretching Rheometer I: Force Balance Analysis", *Rheol. Acta*, 36 (1997) 277-284.
61. Gomez M, Parra I E and Perales J M, "Mechanical Imperfections Effect on the Minimum Volume Stability Limit of Liquid Bridges", *Phys. Fluids*, 14 (2002) 2029-2043.
62. Sanz A, "The Influence of the Outer Bath in the Dynamics of Axisymmetric Liquid Bridges", *J. Fluid Mech.*, 156 (1985) 101-140.
63. Mahajan M P, Tsige M, Taylor P L and Rosenblatt C, "Stability of Liquid Crystalline Bridges", *Phys. Fluids*, 11 (1999) 491-493.
64. Eggers J, "Nonlinear Dynamics and Breakup of Free-Surface Flows", *Rev. Mod. Phys.*, 69 (1997) 865-929.
65. Kröger R, Berg S, Delgado A and Rath H J, "Stretching Behavior of Large Polymeric and Newtonian Liquid Bridges in Plateau Simulation", *J. Non-Newtonian Fluid Mech.*, 45 (1992) 385-400.
66. Nicolás J A, "Hydrodynamic Stability of High-Viscosity Cylindrical Liquid Bridges", *Phys. Fluids A*, 4 (1992) 1620-1626.
67. Yildirim O E and Basaran O A, "Deformation and Breakup of Stretching Bridges of Newtonian and Shear-Thinning Liquids: Comparison of One and Two-Dimensional Models", *Chem. Eng. Sci.*, 56 (2001) 211-233.
68. Zhang X, Padgett R S and Basaran O, "Nonlinear Deformation and Breakup of Stretching Liquid Bridges", *J. Fluid Mech.*, 329 (1996) 207-245.
69. Choi J and Kato T, "Static and dynamic behavior of liquid nano-meniscus bridge", *Tribology Transactions*, 44 (2001) 19-26.
70. Berg S, Kröger R and Rath H J, "Measurement of Extensional Viscosity by Stretching Large Liquid Bridges in Microgravity", *J. Non-Newtonian Fluid Mech.*, 55 (1994) 307-319.
71. McKinley G H and Sridhar T, "Filament Stretching Rheometry of Complex Fluids", in *Annual Review of Fluid Mechanics*, Annual Reviews Press: Palo Alto, (2002) 375-415.
72. Papageorgiou D T, "Analytical Description of the Breakup of Liquid Jets", *Journal of Fluid Mechanics*, 301 (1995) 109-132.
73. Pozrikidis C, "Capillary Instability and Breakup of a Viscous Thread", *J. Eng. Math*, 36 (1999) 255-275.
74. Chen A U, Notz P K and Basaran O A, "Computational and Experimental Analysis of Pinch-Off and Scaling", *Phys. Rev. Lett.*, 88 (2002) 174501-174504.

75. Kowalewski T A, "On the Separation of Droplets from a Liquid Jet", *Fluid Dyn. Res.*, 17 (1996) 121-145.
76. Rothert A, Richter R and Rehberg I, "Transition from Symmetric to Asymmetric Scaling Function Before Drop Pinch-Off", *Phys. Rev. Lett.*, 87 (2001) 4501-4504.
77. Cohen I, Brenner M P, Eggers J and Nagel S R, "Two fluid Drop Snap-Off Problem: Experiments and Theory", *Phys. Rev. Lett.*, 83 (1999) 1147-1150.
78. Doshi P, Cohen I, Zhang W W, Siegel M, Howell P, Basaran O A and Nagel S R, "Persistence of memory in drop breakup: The breakdown of universality", *Science*, 302 (2003) 1185-1188.
79. Burton J C, Rutledge J E and Taborek P, "Fluid Pinch-Off Dynamics at Nanometer Length Scales", *Phys. Rev. Lett.*, 92 (2004) 244505(244504).
80. Yao M, McKinley G H and Debbaut B, "Extensional Deformation, Stress Relaxation and Necking Failure of Viscoelastic Filaments", *J. Non-Newtonian Fluid Mech.*, 79 (1998) 469-501.
81. Koplik J and Banavar J R, "Extensional Rupture of Model non-Newtonian Fluid Filaments", *Phys. Rev. E*, 67 (2003) 011502.
82. Joshi Y M and Denn M M, "Failure and Recovery of Entangled Polymer Melts in Elongational Flow", in *Rheology Reviews 2004* (Binding D M and Walters K, Editors), The British Society of Rheology, Aberystwyth (2004),
83. Hassager O, Kolte M I and Renardy M, "Failure and Nonfailure of Fluid Filaments in Extension", *J. Non-Newtonian Fluid Mech.*, 76 (1998) 137-152.
84. Bazilevskii A V, Entov V M, Lerner M M and Rozhkov A N, "Failure of Polymer Solution Filaments", *Polymer Science Ser. A* (translated from *Vysokomolekulyarnye Soedineniya Ser. A* pp. 474-482), 39 (1997) 316-324.
85. Bazilevskii A V, Entov V M and Rozhkov A N, "Failure of an Oldroyd Liquid Bridge as a Method for Testing the Rheological Properties of Polymer Solutions", *Polymer Science Ser. A* (translated from *Vysokomolekulyarnye Soedineniya Ser. A* pp. 474-482), 43 (2001) 1161-1172.
86. Bazilevsky A V, Entov V M and Rozhkov A N, "Liquid Filament Microrheometer and Some of its Applications", in *Third European Rheology Conference*, (Oliver D R, Editor), Elsevier Applied Science, (1990) 41-43.
87. Anna S L and McKinley G H, "Elasto-capillary Thinning and Breakup of Model Elastic Liquids", *J. Rheol.*, 45 (2001) 115-138.
88. Bechtel S E, Cao J Z and Forest M G, "Practical Application of a higher-order Perturbation Theory for Slender Viscoelastic Jets and Fibers", *J. Non-Newtonian Fluid Mech.*, (1990).

89. Stelter M, Brenn G, Yarin A L, Singh R P and Durst F, "Validation and Application of a Novel Elongational Device for Polymer Solutions", *J. Rheol.*, 44 (2000) 595-616.
90. Liang R F and Mackley M R, "Rheological Characterization of the Time and Strain Dependence for Polyisobutylene Solutions", *J. Non-Newtonian Fluid Mech.*, 52 (1994) 387-405.
91. McKinley G H and Tripathi A, "How to Extract the Newtonian Viscosity from Capillary Breakup Measurements in a Filament Rheometer", *J. Rheol.*, 44 (2000) 653-671.
92. Clasen C, Eggers J, Fontelos M, Li J and McKinley G H, "The "Beads on a String" Structure of Polymeric Jets", *J. Fluid Mech.*, (2005) submitted.
93. Stelter M, Brenn G, Yarin A L, Singh R P and Durst F, "Investigation of the Elongational Behavior of Polymer Solutions by Means of an Elongational Rheometer", *J. Rheol.*, 46 (2002) 507-527.
94. Stelter M, Wunderlich T, Rath S K, Brenn G, Yarin A L, Singh R P and Durst F, "Shear and Extensional Investigations of Solutions of Grafted/Ungrafted Amylopectin and Polyacrylamide", *J. Appl. Polymer Sci.*, 74 (1999) 2773-2782.
95. Wagner C, Amarouchene Y, Doyle P J and Bonn D, "Turbulent Drag Reduction of Polyelectrolyte Solutions; Relation with the Elongational Viscosity", *Eur. Phys. Lett.*, 64 (2003) 823-829.
96. Larson R G, "Constitutive Equations for Polymer Melts and Solutions". Series in Chemical Engineering, ed. H. Brenner, Butterworths, (1988).
97. James D F and Sridhar T, "Molecular Conformation During Steady-State Measurements of Extensional Viscosity", *J. Rheol.*, 39 (1995) 713-724.
98. Kolte M I and Szabo P, "Capillary Thinning of Polymeric Filaments", *J. Rheology*, 43 (1999) 609-626.
99. Rodd L E, Scott T P, Cooper-White J J and McKinley G H, "Capillary Breakup Rheometry of Low-Viscosity Elastic Fluids", *Appl. Rheol.*, 15 (2005) 12-27.
100. Bhattacharjee P K, Oberhauser J P, McKinley G H, Leal L G and Sridhar T, "Extensional Rheometry of Entangled Solutions", *Macromolecules*, 25 (2002) 10131-10148.
101. Bhattacharjee P K, Nguyen D A, McKinley G H and Sridhar T, "Extensional Stress Growth and Stress Relaxation in Entangled Polymer Solutions", *J. Rheol.*, 47 (2003) 269-290.
102. Yao M, Spiegelberg S H and McKinley G H, "Fluid Dynamics of Weakly Strain-Hardening Fluids in Filament Stretching Devices", *J. Non-Newtonian Fluid Mech.*, 89 (2000) 1-43.

103. McKinley G H, Brauner O and Yao M, "Kinematics of Filament Stretching in Dilute and Concentrated Polymer Solutions", *Korea-Aust. Rheol. J.*, 13 (2001) 29-35.
104. Joseph D D, "Fluid Dynamics of Viscoelastic Liquids". Series in Applied Mathematics, Springer-Verlag, (1990).
105. Hupp S, Personal Communication, (2005).
106. Doshi P and Basaran O A, "Self-similar pinch-off of power law fluids", *Phys. Fluids*, 16 (2004) 585-593.
107. Doshi P, Suryo R, Yildirim O E, McKinley G H and Basaran O A, "Scaling in Pinch-Off of Generalized Newtonian Fluids", *J. Non-Newtonian Fluid Mech.*, 113 (2003) 1-27.
108. Park A E, "Capillary Breakup of Food Stuffs and Other Complex Fluids", MS Thesis, MIT, Cambridge (USA), (2003)
109. Goldin M, Pfeffer R and Shinnar R, "Breakup of a Capillary Jet of a Non-Newtonian Fluid Having a Yield Stress", *Chem. Eng. J.*, 4 (1971) 8-21.
110. Shore H J and Harrison G, "The Effect of Added Polymer on the Formation of Drops Ejected from a Nozzle", *Phys. Fluids*, 17 (2005) 033104.
111. Funada T and Joseph D D, "Viscoelastic Potential Flow Analysis of Capillary Instability", *J. Non-Newtonian. Fluid Mech.*, 111 (2003) 87-101.
112. Wang J, Joseph D D and Funada T, "Purely Irrotational theories of the Effects of Viscosity and Viscoelasticity on Capillary Instability of a Liquid Cylinder", *J. Non-Newtonian. Fluid Mech.*, (2005) in press.
113. Puchelle E, Zahm J M and Duvivier C, "Spinability of Bronchial Mucus. Relationship with Viscoelasticity and Mucous Transport Properties", *Biorheology*, 20 (1983) 239-249.
114. Zahm J M, Puchelle E, Duvivier C and Didelon J, "Spinability of Respiratory Mucus. Validation of a New Apparatus: The Filancemeter", *Bull. Eur. Physiopathol. Respir.*, 22 (1986) 609-613.
115. Glover F A and Scott-Blair G W, "The Flow Properties of Cervical Secretions in the Cow as Related to Certain Physiological Conditions", *J. Endocr.*, 9 (1953) 160-180.
116. Kopito L E and Kosasky H J, "The Tackiness Rheometer determination of the Viscoelasticity of Cervical Mucus", in *Human Ovulation*, (Hafez E S F, Editor), Elsevier/North-Holland, Amsterdam, (1979), 351-361.
117. James D F. "An Extensional Viscosity for Fluid Breakup", 75th Annual Meeting of the Society of Rheology, Pittsburgh, PA (USA), Paper ER4, 2003.
118. Pitois O, Moucheron P and Chateau X, "Liquid Bridge Between Two Moving Spheres: An Experimental Study of Viscosity Effects", *J. Coll. Int. Sci.*, 231 (2000) 26-31.

119. Craster R V, Matar O K and Papageorgiou D T, "Pinchoff and Satellite Formation in Surfactant-Covered Viscous Threads", *Phys. Fluids*, 14 (2002) 1364-1376.
120. Liao Y C, Subramani H J, Franses E I and Basaran O A, "Effects of Soluble Surfactants on the Deformation and Breakup of Stretching Liquid Bridges", *Langmuir*, 20 (2004) 9926-9930.
121. Rothstein J P, "Transient Extensional Rheology of Wormlike Micelle Solutions", *J. Rheol.*, 47 (2003) 1227-1247.